

DTIC FILE COPY

AD-A188 577

Nab. Defense
Defence nationale



DTIC
ELECTE
DEC 17 1987
S D

AN ANALYSIS OF DREO's ANALOG REBALANCE LOOPS FOR THE CSG-2 TUNED-ROTOR GYROSCOPE

by

Jeffrey Bird

DISTRIBUTION STATEMENT

Approved for public release,
Distribution Unlimited

DEFENCE RESEARCH ESTABLISHMENT OTTAWA

TECHNICAL NOTE 87-15

Canada

July 1987
Ottawa

87 12 10 038



National
Defence

Défense
nationale

AN ANALYSIS OF DREO's ANALOG REBALANCE LOOPS FOR THE CSG-2 TUNED-ROTOR GYROSCOPE

by

Jeffrey Bird
*Electromagnetics Section
Electronics Division*

Accession For	
NTIS CRA&I	<input checked="" type="checkbox"/>
DTIC TAB	<input type="checkbox"/>
Unannounced	<input type="checkbox"/>
Justification	
By	
Distribution /	
Availability Codes	
Dist	Avail and/or Special
A-1	



DEFENCE RESEARCH ESTABLISHMENT OTTAWA
TECHNICAL NOTE 87-15

PCN
041LJ

July 1987
Ottawa

ABSTRACT

The Defence Research Establishment Ottawa (DREO) designed and constructed a high performance analog rebalance loop for the Canadian Strapdown Gyroscope (CSG-2). This instrument is a potentially low cost, near inertial grade, two degree-of-freedom, tuned-rotor gyro designed and manufactured by Litton Systems Canada Ltd. under contract to DREO. The resulting loops are analyzed extensively from a control systems point of view with the examination of such properties as closed-loop stability, frequency and time responses and, to some extent, stability margin, as interpreted from multivariable generalizations of classical control-theoretic notions of Nyquist plots and root loci. The results indicate that the loops will provide sufficient closed-loop performance to achieve the desired goals of bandwidth, maximum input rate, low cross-axis coupling and acceleration compensation.

RÉSUMÉ

Le Centre de recherches pour la défense/Ottawa (CRDO) a conçu et fabriqué une boucle analogique de rétablissement d'équilibre très performante pour le Gyroscope canadien à composants liés (CSG-2). Ce dispositif quasi inertiel, à deux degrés de liberté, à rotor accordé et dont la fabrication pourra peut-être exiger peu de frais, a été conçu et fabriqué par Litton Systems Canada Ltd. pour le compte du CRDO. Les boucles réalisées sont analysées à fond du point de vue des systèmes de commande, en particulier en ce qui a trait aux propriétés de stabilité en boucle fermée, de réponse temporelle et en fréquence et, jusqu'à un certain point, la marge de stabilité, par l'interprétation des généralisations multivariables des concepts classiques de contrôle des variables théoriques des diagrammes de Nyquist et des lieux des racines. Les résultats indiquent que la performance en boucle fermée de ces dispositifs permettra d'obtenir les caractéristiques nécessaires, du point de vue de la largeur de bande, du débit d'entrée minimal, du faible couplage entre les axes et de la compensation d'accélération.

CONTENTS

ABSTRACT	iii
RÉSUMÉ	v
CONTENTS	vii
FIGURES	ix
TABLES	xi
1 INTRODUCTION	1
2 SYSTEM MODELLING	3
2.1 Simple Gyro Model	3
2.2 Rebalance Loop Models	5
2.3 Closed-Loop Equations	8
2.3.1 Frequency Domain Descriptions	8
2.3.2 State Space Description	10
3 ANALYSIS SOFTWARE	12
4 SUMMARY OF RESULTS	12
4.1 Stability	13
4.2 Time Domain Simulations	17
4.2.1 Step Responses	18
4.2.2 Steady-State Results	25
4.2.3 Roll Rate Tests	27
4.3 Frequency Domain Characteristics	31
4.3.1 Closed-Loop Frequency Response	31
4.3.2 The Sensitivity Function	34
4.3.3 Nyquist Plots	39
4.4 Effects Of A Better Gyro Model	47
5 CONCLUSIONS	48
6 RECOMMENDATIONS	49
REFERENCES	50
APPENDICES	
A LIST OF COMPENSATOR PARAMETERS	51

FIGURES

Fig.	Title	Page
1	The closed-loop system	9
2a	RL-2 root locus varying p_1	16
2b	RL-3 root locus varying p_1	16
3	Root locus of special case $C=(p_8)Ds^{\sim}$ varying p_8	17
4a	RL-2 step rate response (outputs)	20
4b	RL-3 step rate response (outputs)	20
5a	RL-2 step rate response (pickoffs)	21
5b	RL-3 step rate response (pickoffs)	21
6a	RL-2 step acceleration response (outputs)	22
6b	RL-3 step acceleration response (outputs)	22
7a	RL-2 step acceleration response (cross-axis)	23
7b	RL-3 step acceleration response (cross-axis)	23
8a	RL-2 step acceleration response (pickoffs)	24
8b	RL-3 step acceleration response (pickoffs)	24
9	Roll test, input position profile = $-\phi_{cx}$	28
10	Roll test, input rate profile = $-\omega_{cx}$	28
11a	RL-2 roll error = $-\phi_{cx} - \int OUT^x$	29
11b	RL-3 roll error = $-\phi_{cx} - \int OUT^x$	29
12a	RL-2 roll test, integrated cross-axis output = $\int OUT^y$	30
12b	RL-3 roll test, integrated cross-axis output = $\int OUT^y$	30
13a	RL-2 closed-loop frequency response, magnitude & phase	32
13b	RL-3 closed-loop frequency response, magnitude & phase	33
14a	RL-2 sensitivity functions	36
14b	RL-3 sensitivity functions	36
15a	RL-2 maximum singular value sensitivity function	38
15b	RL-3 maximum singular value sensitivity function	38
16	Nyquist "D-contour"	40
17	System with one loop open	41
18a	RL-2 Nyquist plot	43
18b	RL-3 Nyquist plot	43
19a	RL-2 Nyquist plot, gain increased to $p_1=.27$	44
19b	RL-3 Nyquist plot, gain increased to $p_1=.46$	44
20a	RL-2 Nyquist plot, added phase of 37 degrees	45
20b	RL-3 Nyquist plot, added phase of 48 degrees	45

TABLES

Table	Title	Page
1	Nominal closed-loop pole locations	13
2	Results of root locus tests	17
3	Steady-state values	27
4	Stability margins	46

1 INTRODUCTION

This report summarizes the results of an extensive study of some major control-theoretic aspects of a particular gyroscope/ rebalance loop configuration. The gyro was designed by Litton Systems Canada and is similar to previous generations of two degree-of-freedom, dry, tuned-rotor gyroscopes [1] except for the way the flexures are made and machined into the gimbals. These innovations have resulted in the potential to produce a good quality gyro at a cost lower than current comparable devices. Preliminary testing at the Defence Research Establishment Ottawa (DREO) inertial navigation laboratory has been very encouraging and indicates that this instrument may be very near to inertial grade quality. A summary of the gyro's innovative features and the preliminary test results may be found in [2].

Since the gyro was designed for strapdown applications, a suitable electronic rebalance loop must be designed to keep the rotor aligned with the gyro case as it rotates with the vehicle it is strapped to. The loop receives signals from the gyro's pickoff circuitry that indicate the angular displacement of the rotor with respect to the case in two axes. The loop supplies currents to the gyro's torquer coils that, through magnetic interaction, apply a torque to the rotor causing it to precess at a certain rate in a particular direction. If the loop is designed properly, the rotor will stay more or less aligned to the case at all times, and a measurement of the rate applied to the case is available by measuring the current supplied to the torquer coils.

Though simple in concept, the design of suitable rebalance loops has proven to be a nontrivial problem. In particular, it is a two-input, two-output control problem so it is difficult to apply classical single-input, single-output control design techniques directly. To do so naively would generally result in

a closed-loop system that has high interaction (a rate on one input axis of the gyro produces a non-negligible output reading on the other axis). In addition, the traditional tradeoffs of tracking versus stability margin and bandwidth versus noise rejection have to be addressed.

Rebalance loop designs can be divided into two major groups - analog and digital. The digital designs are attractive since they directly produce digital data for the system computer. It can be argued, however, that for high accuracy applications, analog loops are better. Unfortunately, the analog information must be converted to digital form for the computer and this is a difficult problem. That, however, is beyond the scope of this study. Each of the preceding categories can be divided into schemes that employ "cross-axis compensation" and those that do not. Cross-axis compensation attempts to eliminate or reduce the interaction between the two axes of the gyro. Without it, the loop can be designed as if there were two single-input, single-output loops. However the results are better if the inherent multivariable nature of the system is taken into consideration.

Several research groups are currently studying various rebalance loop techniques for the CSG-2. DREO [3] has developed a high performance analog rebalance loop (with and without cross-axis compensation) to enable the inertial navigation lab to make accurate performance tests of the CSG-2. Such a scheme can then be evolved into any end-use system that employs this gyro. It is the purpose of this report to analyze the DREO rebalance loops and the gyro as a closed-loop control system. This was done by studying the expected responses of the system (in both time and frequency domains) and calculating various measures of performance (tracking errors, sensitivity, robustness, etc.). Extensive simulation software was developed to do this. No attempt was made to model the expected but unpredictable effects in the system, such as thermal effects in both the gyro and rebalance loop, random gyro drifts, etc. Such

effects can best be determined experimentally and will be done so upon completion of the loops; this will be the subject of subsequent DREO studies.

2 SYSTEM MODELLING

This section is a summary of the system models that were used during the design and analysis of the rebalance loops. Most of the derivations are omitted for brevity.

2.1 Simple Gyro Model

A complete description of a typical tuned-rotor gyro is very complex. For an exhaustive treatment of the subject, the reader is referred to [4],[5]. In those papers, there are several models of the gyro one can use depending on the degree of accuracy required. For example, during gyro construction, it may be important to know the effects of asymmetry in the flexure spring constants. For the purposes of this study, however, a very simple gyro model was used. This is justified because a stable, closed-loop control system is generically robust with respect to slight variations in the open-loop plant dynamics (eg. classical gain/phase margins). Though this is not true for multivariable, open-loop unstable systems [6], it is true for the CSG-2 as it is open-loop stable.

The ideal tuned-rotor gyro is symmetric with respect to its two input axes, has negligible internal damping forces, and is running at exactly tuned speed. Then, all internal spring forces "balance out" and the rotor will remain stationary in inertial space should the case rotate about it and no rebalance loop were in place.

The equations of motion for the gyro are

$$\theta_x(s) = -\frac{1}{s} \omega_{cx} + \frac{I}{H^2} \left[\frac{T_x(s) - \frac{H}{sI} T_y(s)}{1 + \left(\frac{sI}{H}\right)^2} \right]$$

$$\theta_y(s) = -\frac{1}{s} \omega_{cy} + \frac{I}{H^2} \left[\frac{T_y(s) + \frac{H}{sI} T_x(s)}{1 + \left(\frac{sI}{H}\right)^2} \right]$$

or in matrix notation

$$\begin{bmatrix} \theta_x(s) \\ \theta_y(s) \end{bmatrix} = -\frac{1}{s} \begin{bmatrix} \omega_{cx}(s) \\ \omega_{cy}(s) \end{bmatrix} + \frac{I/H^2}{1 + \left(\frac{sI}{H}\right)^2} \begin{bmatrix} 1 & -H/sI \\ H/sI & 1 \end{bmatrix} \begin{bmatrix} T_x(s) \\ T_y(s) \end{bmatrix}$$

where

s is the Laplace variable,

H is the angular momentum of the rotor,

I is the moment of inertia of the rotor about
an axis through the plane of the rotor,

T_x, T_y are torquer currents produced by the rebalance loop,

ω_{cx}, ω_{cy} are the angular rates applied to the gyro case,

θ_x, θ_y are the pickoff angles sensed by the rebalance
loop.

Note that an important constant that appears in the above equations is (H/I) . This term defines a natural frequency, called the "nutation frequency" of the gyro and for the CSG-2, this is 165. Hertz or 1036.7255 radians/sec. Let the nutation frequency be

$$\omega_n := H/I = 1036.7255 \text{ rad/s.}$$

(The symbol $:=$ or $=:$ denotes a definition.) To normalize the model, one can define

$$s^- := s/\omega_n = sI/H$$

and absorb a factor of $1/H$ into the torquer current terms, T_x and T_y . This is realistic because these terms are included in the gyro's "torquer scale factor", a constant that represents the conversion of current to a rotation rate of the rotor due to the torquer coils. The model of the gyro in the frequency domain then becomes (dropping the implied functional dependence on s)

$$\begin{bmatrix} \theta_x \\ \theta_y \end{bmatrix} = -\frac{1}{s} \begin{bmatrix} \omega_{cx} \\ \omega_{cy} \end{bmatrix} + \frac{1/\omega_n}{\tilde{s}^2 + 1} \begin{bmatrix} 1 & -1/\tilde{s} \\ 1/\tilde{s} & 1 \end{bmatrix} \begin{bmatrix} T_x \\ T_y \end{bmatrix}.$$

If ϕ_{rx} and ϕ_{ry} are defined as the absolute angular positions of the rotor:

$$\begin{aligned} \begin{bmatrix} \phi_{rx} \\ \phi_{ry} \end{bmatrix} &:= \frac{1}{\tilde{s}^2 + 1} \begin{bmatrix} 1 & -1/\tilde{s} \\ 1/\tilde{s} & 1 \end{bmatrix} \begin{bmatrix} T_x \\ T_y \end{bmatrix} \\ &=: P(s) \begin{bmatrix} T_x \\ T_y \end{bmatrix} \end{aligned}$$

and the factor of $1/\omega_n$ is ignored (this will be absorbed into the gain term of the compensator), then a very compact frequency domain description of the open-loop gyro results:

$$\begin{bmatrix} \theta_x \\ \theta_y \end{bmatrix} = -\frac{1}{s} \begin{bmatrix} \omega_{cx} \\ \omega_{cy} \end{bmatrix} + P \begin{bmatrix} T_x \\ T_y \end{bmatrix}. \quad (1)$$

2.2 Rebalance Loop Models

The rebalance loop consists of a 2 by 2 transfer function matrix with input pickoff signals, θ_x and θ_y , and output torquer currents, T_x and T_y . In general terms, this is

represented by

$$\begin{bmatrix} T_x(s) \\ T_y(s) \end{bmatrix} = \begin{bmatrix} -C(s) & -D(s) \\ D(s) & -C(s) \end{bmatrix} \begin{bmatrix} \theta_x(s) \\ \theta_y(s) \end{bmatrix} \\ =: K(s) \begin{bmatrix} \theta_x(s) \\ \theta_y(s) \end{bmatrix} \quad (2)$$

where $D(s)$ represents the "direct-axis" compensation and $C(s)$ is the "cross-axis" compensation, so named because a torque applied on the x-axis has a much stronger effect on the y-pickoff angle than on the x. The outputs of the rebalance loop are taken as the torquer currents since they provide a measure of the torque required to realign the rotor with the case, and hence a measure of the applied case rate. The outputs are not the total torquer currents, however, only the portion due to the direct-axis compensation:

$$\begin{bmatrix} \text{OUT}_x(s) \\ \text{OUT}_y(s) \end{bmatrix} := \begin{bmatrix} D(s) & 0 \\ 0 & D(s) \end{bmatrix} \begin{bmatrix} \theta_x(s) \\ \theta_y(s) \end{bmatrix} \quad (3)$$

DREO has developed two rebalance loop schemes dubbed RL-2 and RL-3 [3] and has applied for a patent on the designs (DND invention 1416-86-001). The first, RL-2, has no cross-axis compensation so $C(s)=0$. The direct-axis term, $D(s)$, consists of an integrator and a fourth-order, low-pass filter. Thus,

$$\text{RL-2} : D(s) = G_1(s)G_2(s)G_3(s) ; \quad C(s) = 0.$$

where, in the notation of [3],

$$G_1(s) = p_1 \left(1 + \frac{p_2}{s} \right)$$

$$G_2(s) = \frac{p_3^2}{s^2 + 2p_3p_4s + p_3^2}$$

$$G_3(s) = \frac{p_6^2}{s^2 + 2p_6p_7s + p_6^2}$$

For a complete list of the parameters of $D(s)$, the reader is referred to Appendix A. Reference [3] describes in detail the process by which the parameters were chosen. The basic approach was to vary the parameters until the frequency response of the closed-loop direct-axis transfer function had a fairly smooth magnitude response (and a suitably high bandwidth) and good phase response characteristics for a degree of stability margin. In RL-2, there was no consideration given to the closed-loop cross-axis transfer function so a relatively large degree of interaction was expected.

The second loop, RL-3, employs the cross-axis term, $C(s)$.

$$\text{RL-3: } D(s) = G_1(s)G_2(s)G_3(s)G_4(s);$$

$$C(s) = G_1(s)G_2(s)G_4(s)G_5(s)G_6(s)$$

where G_1 , G_2 , and G_3 are as above and,

$$G_4(s) = \frac{s^2 + 2p_5p_f p_e s + p_e^2}{s^2 + 2p_f p_e s + p_e^2} \quad (\text{spin notch filter})$$

$$G_5(s) = p_8 s \frac{p_c^2}{s^2 + 2p_d p_c s + p_c^2}$$

$$G_6(s) = \frac{s^2 + 2p_a p_9 p_b s + p_9^2}{s^2 + 2p_9 p_b s + p_9^2}$$

Again, a complete list of the parameters is given in

Appendix A. Note that the functions, $G_i(s)$, are not necessarily the same in RL-2 and RL-3. Note also that p_1 is the principle gain term in the compensator; this is the term that absorbed the $1/\omega_n$ from the plant model. The design procedure for RL-3 was essentially the same as that for RL-2 except the cross-axis closed-loop function was also considered. In the next section, it will be seen that perfect decoupling (that is, zero interaction between the two gyro axes) can be obtained if $C(s) = s \tilde{D}(s)$. However, this is not an acceptable solution as Section 4.1 will note that this would result in an imaginary axis pole - zero cancellation in the closed-loop transfer function, causing internal oscillations and hence instability (in modern control theory terms, this is an unobservable unstable mode). The idea behind the design of the cross-axis compensator in RL-3 was to make $C(s)$ approximately equal to $s \tilde{D}(s)$ at low frequencies (over the bandwidth of the instrument) to provide near perfect decoupling at these frequencies, but to make $C(s)$ sufficiently different from $s \tilde{D}(s)$ at higher frequencies to provide stability. An additional benefit of RL-3 is that it provides "cross-axis acceleration cancellation", a concept described later.

2.3 Closed-Loop Equations

2.3.1 Frequency Domain Descriptions

The previous section established the two primary equations of the system, equations (1) and (2). From these, the closed-loop system can be drawn as in Figure 1 below. Abbreviate notation slightly and define

$$\omega_c := \begin{bmatrix} \omega_{cx} \\ \omega_{cy} \end{bmatrix}, \quad \theta := \begin{bmatrix} \theta_x \\ \theta_y \end{bmatrix}, \quad T := \begin{bmatrix} T_x \\ T_y \end{bmatrix}, \quad \text{OUT} := \begin{bmatrix} \text{OUT}_x \\ \text{OUT}_y \end{bmatrix}, \quad \phi_r := \begin{bmatrix} \phi_{rx} \\ \phi_{ry} \end{bmatrix}.$$

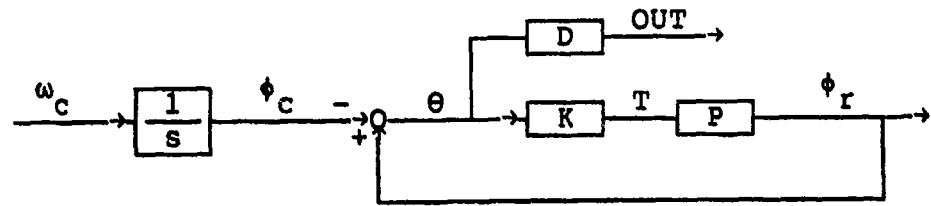


Fig. 1: The closed-loop system

The resulting loop looks very much like a classical feedback system except that it must be remembered that each of the signal lines is actually a vector of 2 signals and each block is a 2 by 2 transfer matrix. The closed-loop equations are developed with standard matrix algebra:

$$\begin{aligned}
 \theta &= -\phi_c + \phi_r \\
 &= -\phi_c + PK\theta \\
 \rightarrow [I_2 - PK]\theta &= -\phi_c \\
 \rightarrow \theta &= -[I_2 - PK]^{-1} \phi_c \\
 &= -1/s [I_2 - PK]^{-1} \omega_c \\
 \rightarrow \text{OUT} &= -D/s [I_2 - PK]^{-1} \omega_c
 \end{aligned}
 \tag{4}$$

where I_2 is the 2 by 2 identity matrix. Recall that $D(s)$ has an extra factor of $1/\omega_n$ in it as a result of normalizing the plant. This is why s is also multiplied by $1/\omega_n$ in equation (5).

It is these equations upon which much of the subsequent analysis is based. If the matrices of P and K are substituted into (5) and the operations carried out, the closed-loop transfer functions are obtained:

$$\begin{bmatrix} \text{OUT}_x \\ \text{OUT}_y \end{bmatrix} = \frac{-D}{(\tilde{s}^2 + C)^2 + (\tilde{s} + D)^2} \begin{bmatrix} \tilde{s}(\tilde{s}^2 + C + 1) + D & -D\tilde{s} + C \\ D\tilde{s} - C & \tilde{s}(\tilde{s}^2 + C + 1) + D \end{bmatrix} \begin{bmatrix} \omega_{cx} \\ \omega_{cy} \end{bmatrix}. \quad (6)$$

As noted in the previous section, if $C = D\tilde{s}$ then the closed-loop cross-axis function is clearly 0 but if $C = D\tilde{s}$ is substituted in the direct loop, it can be shown that there will be a pole - zero cancellation at $\tilde{s} = \pm j1$, (i.e. a closed-loop pole on the imaginary axis at $s = \pm j\omega_n$) indicating a destabilizing compensator.

2.3.2 State Space Description

It was convenient to express the system models in a state space form (see any text on modern control theory). This involves the formation of a vector x and matrices A , B , E of appropriate dimensions so that the equations

$$\begin{aligned} \dot{x} &= [A]x + [B]u \\ y &= [E]x \end{aligned}$$

describe the time domain dynamic behavior between the input vector u and the output vector y .

The nominal gyro model has a very simple state space representation. Take the input vector, u , as the torquer currents, T . The output vector, y , and the state vector, x , are both defined as the absolute angular rates of the rotor, ω_r . The measured output vector (the pickoff angle, θ), is the integral of the difference between the rotor angular rate, ω_r , and the case angular rate, ω_c . Hence,

$$\left. \begin{aligned} \dot{x} &= [A]x + [B]T \\ \omega_r &= [E]x \\ \dot{\theta} &= -\omega_c + \omega_r \end{aligned} \right\} \quad (7)$$

where

$$\omega_r = \text{Rotor angular rate} = \begin{bmatrix} \omega_{rx} \\ \omega_{ry} \end{bmatrix} = \begin{bmatrix} \dot{\phi}_{rx} \\ \dot{\phi}_{ry} \end{bmatrix}$$

$$[A] = \begin{bmatrix} 0 & -\omega_n \\ \omega_n & 0 \end{bmatrix}, \quad [B] = \begin{bmatrix} \omega_n & 0 \\ 0 & \omega_n \end{bmatrix}, \quad [E] = \begin{bmatrix} 1 & 0 \\ 0 & 1 \end{bmatrix}.$$

The Laplace transform of this model is exactly the frequency domain model of the gyro, equation (1).

The state space matrix of the rebalance loop is much larger than that of the gyro so for brevity it is omitted. It is a simple controllable canonical form of the transfer function of the loop with the appropriate interconnections. It has up to 22 states (for RL-3), has two inputs and two outputs, and will simply be expressed as

$$\begin{aligned} \dot{z} &= [\Phi]z + [\Psi]\theta \\ T &= [\Gamma]z \end{aligned} \quad \} \quad (8)$$

where the matrices Φ , Ψ , and Γ are of dimensions 22 by 22, 22 by 2, and 2 by 22 respectively. The augmentation of systems (7) and (8) results in the following closed-loop state space description:

$$\left. \begin{aligned} \begin{bmatrix} \dot{x} \\ \dot{z} \\ \dot{\theta} \end{bmatrix} &= \begin{bmatrix} A & B\Gamma & 0 \\ 0 & \Phi & \Psi \\ E & 0 & 0 \end{bmatrix} \begin{bmatrix} x \\ z \\ \theta \end{bmatrix} + \begin{bmatrix} 0 \\ 0 \\ -I_2 \end{bmatrix} \begin{bmatrix} \omega_{cx} \\ \omega_{cy} \end{bmatrix} \\ \theta &= \begin{bmatrix} 0 & 0 & I_2 \end{bmatrix} \begin{bmatrix} x \\ z \\ \theta \end{bmatrix} \end{aligned} \right\} \quad (9)$$

The system in this form (which is the time domain equivalent of the frequency domain description (6)) is more amenable to computer simulations. Time domain simulations are simple with a general differential equation solving program and closed-loop stability can be determined at a glance from the

eigenvalues of the closed-loop state dynamic matrix (the eigenvalues are exactly the closed-loop poles).

3 ANALYSIS SOFTWARE

Extensive software was written to simulate the models discussed in the previous section. Various frequency domain properties of the closed-loop system could be examined from equation (5) such as frequency responses, sensitivity, and an attempt at multivariable Nyquist plots. Closed-loop time responses are available from the propagation of equation (9) for arbitrary rate inputs. Stability is determined from the eigenvalues of the closed-loop state space matrix. Root locus plots are also made by finding closed-loop pole locations as a function of some parameter.

Since commercial software for eigenvalues or differential equations was not immediately available at the time of the study, educational software routines were adapted to perform these functions. Consequently the programs are not guaranteed to be efficient, though they are quite accurate.

Some of the analysis software, particularly for the frequency domain calculations, was expanded to incorporate a more complex dynamic model of the gyro which included internal damping and time constant terms. This is examined briefly in a later section.

4 SUMMARY OF RESULTS

This section summarizes the major results of the study. First, stability was verified by the location of the closed-loop poles of the nominal system and the examination of

root locus plots - the locus of the poles as a particular parameter is changed. This gives some indication of sensitivity to gain variations. Next, several time response simulations were conducted and the most visible differences between RL-2 and RL-3 can be seen from these. Time domain steady-state responses were calculated from the closed-loop transfer functions and an application of the final value theorem. Various frequency domain properties were calculated, including closed-loop responses, Nyquist and sensitivity plots, and an attempt at their interpretation is given.

4.1 Stability

The eigenvalues of the closed-loop state dynamic matrix of Section 2.3.2 (eq. 9) immediately indicate the stability of the system. Table 1 lists the closed-loop poles of the nominal systems for both the RL-2 and RL-3 configurations. All the poles must lie in the left half of the complex s-plane, $\{s: \text{Re } s < 0\}$, for stability. From the table, this is evident as all real parts are negative.

Table 1: Nominal closed-loop pole locations

RL-2

EIGENVALUES OF CLOSED-LOOP MATRIX

Real part	Imaginary part
-97.20	1082.46
-97.20	-1082.46
-991.70	944.55
-991.70	-944.55
-861.65	952.70
-861.65	-952.70

-701.75	324.55
-701.75	-324.55
-96.01	487.26
-96.01	-487.26
-199.76	200.63
-199.76	-200.63
-37.53	0.32
-37.53	-0.32

RL-3

EIGENVALUES OF CLOSED-LOOP MATRIX

Real part

Imaginary part

Real part	Imaginary part
-1152.12	1591.93
-1152.12	-1591.93
-1197.68	1466.09
-1197.68	-1466.09
-139.54	1259.83
-139.54	-1259.83
-496.29	1175.13
-496.29	-1175.13
-1062.68	600.50
-1062.68	-600.50
-89.99	885.03
-89.99	-885.03
-600.96	789.71
-600.96	-789.71
-59.64	669.37
-59.64	-669.37
-46.15	670.55
-46.15	-670.55
-615.28	108.96
-615.28	-108.96
-247.55	402.29
-247.55	-402.29
-235.95	379.70
-235.95	-379.70
-37.20	1.25E-04
-37.20	-1.25E-04

First, notice that RL-3 has many more poles than RL-2

because of the cross-axis compensation and a spin notch filter (G_4) that was added to each loop of RL-3 to reduce some of the noise introduced by the spin motor. It is difficult to tell "how stable" the two configurations are by pole locations. The poles that appear the "least stable" are the ones at approximately $(-37 \pm j0)$ because they are closest to the imaginary axis of the s-plane.

However, a feel for stability is obtained by a simple multivariable gain margin. For single-loop systems, recall, the gain margin is the amount of pure gain that can be added to the open-loop system before the closed-loop becomes unstable. This system is a multi-loop configuration and it is not clear how to determine a suitable measure of gain margin. (See [6] and the references therein for current research in the area.) One method is to simply change the gain of the open-loop system (by changing the coefficient p_1 in the compensator model) and check stability by the location of the closed-loop poles. This is a direct multi-loop generalization of classical "root locus" plots. Figures 2a and 2b show the location of the poles of the two configurations as p_1 increases from its nominal value to a destabilizing value, indicated by a pole crossing to the right half plane. Each pole is shown with an arrow indicating its direction of travel as p_1 increases. The large dot on each locus indicates the pole location for the nominal value of p_1 , approximately 0.2. Note that only the upper half of the s-plane is shown. There is a symmetric set of poles in the lower half plane due to their complex conjugate nature. These plots were software generated, as the well known rules for constructing the root locus of single-loop systems do not carry over to the multi-loop case. The results of this test are indicated in Table 2.

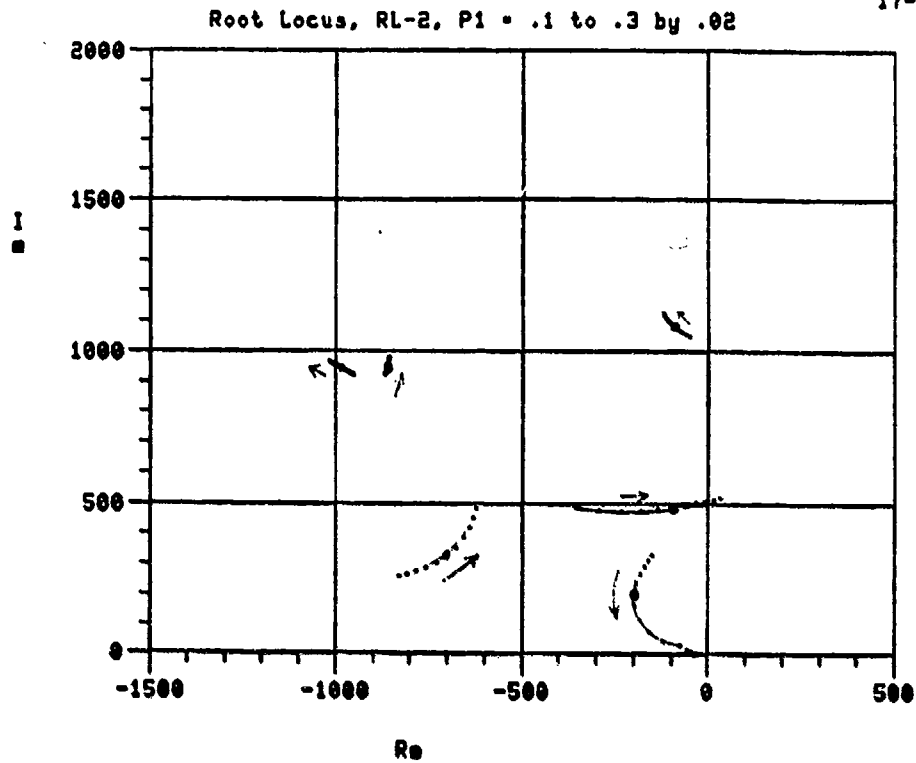
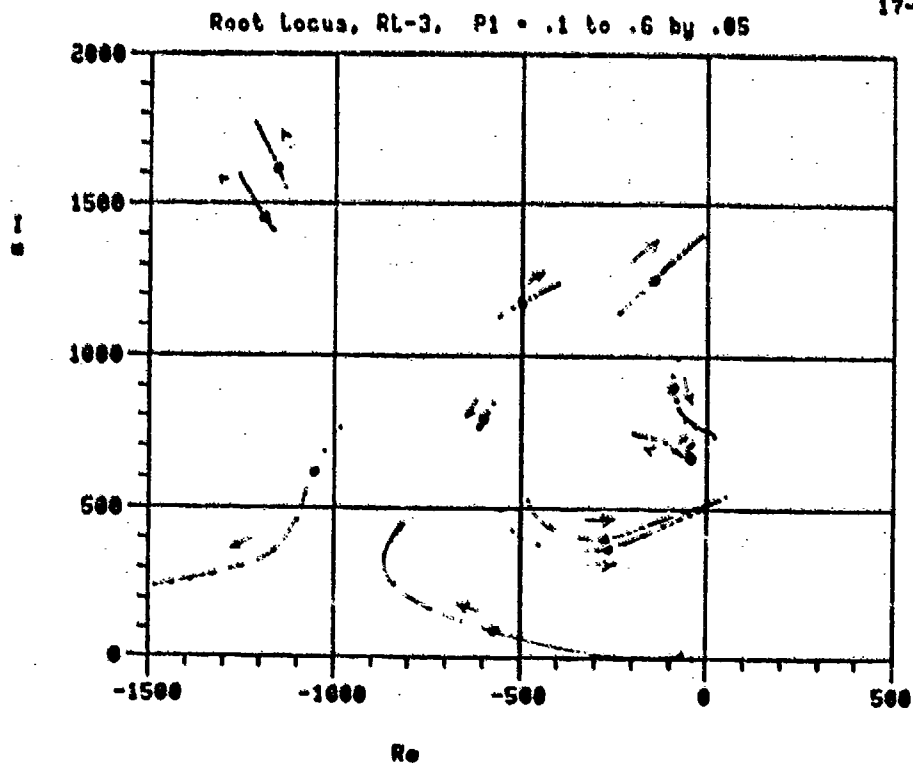
UAX GPLOT
17-DEC-85Fig. 2a: RL-2 root locus varying p_1 UAX GPLOT
17-DEC-86Fig. 2b: RL-3 root Locus varying p_1

Table 2: Results of root locus tests

Loop	Nominal gain	Destabilizing gain
RL-2	$p_1 = 0.2$	$p_1 = 0.27$
RL-3	$p_1 = 0.21$	$p_1 = 0.46$

Table 2 indicates that the gain in RL-2 can be increased 35% (2.6 db) and that of RL-3 can be increased by 120% (6.8 db) before the system is unstable. Both are good margins but obviously RL-3 is better.

The root locus plot of a special case of RL-3 was briefly examined. As noted in a previous section, if $C(s) = s\tilde{D}(s)$, perfect cross-axis decoupling would result but the closed-loop would have imaginary axis poles. This is demonstrated with an appropriate choice of compensator parameters so that $C(s) = (p_g)s\tilde{D}(s)$ with p_g varied around 1.0. The list of parameters used in this test can be found in Appendix A. The resulting root locus plot is shown in Figure 3. Indeed, a pole does cross to the right half plane as p_g exceeds 1.0 verifying that the system is marginally unstable for $C(s) = s\tilde{D}(s)$.

4.2 Time Domain Simulations

Simulations of the closed-loop systems for various input case rates were conducted by numerically integrating the set of differential equations (9) with a fourth order Runge-Kutta algorithm. In all examples, the y case rate is set to zero, so the direct-axis response is indicated by the x-outputs and the cross-axis response is shown by the y-outputs. For inputs on the y case axis, the results are identical except for the sign of the cross-axis response.

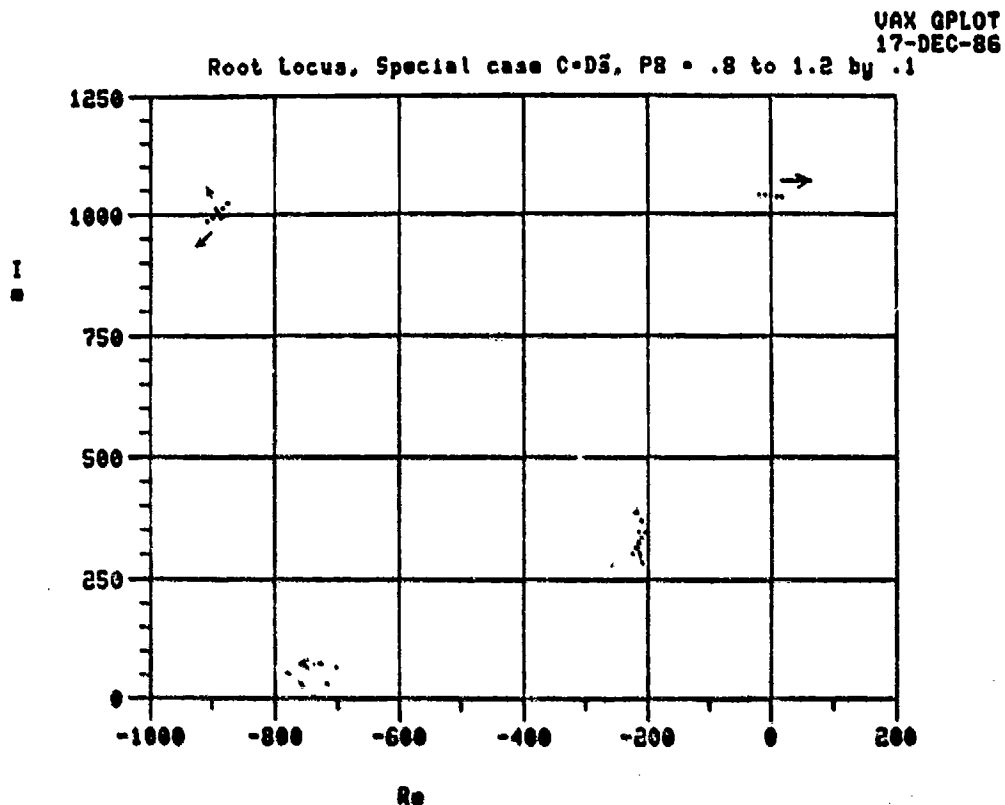


Fig. 3: root locus of special case $C=(p_8)D\ddot{s}$, varying p_8

4.2.1 Step Responses

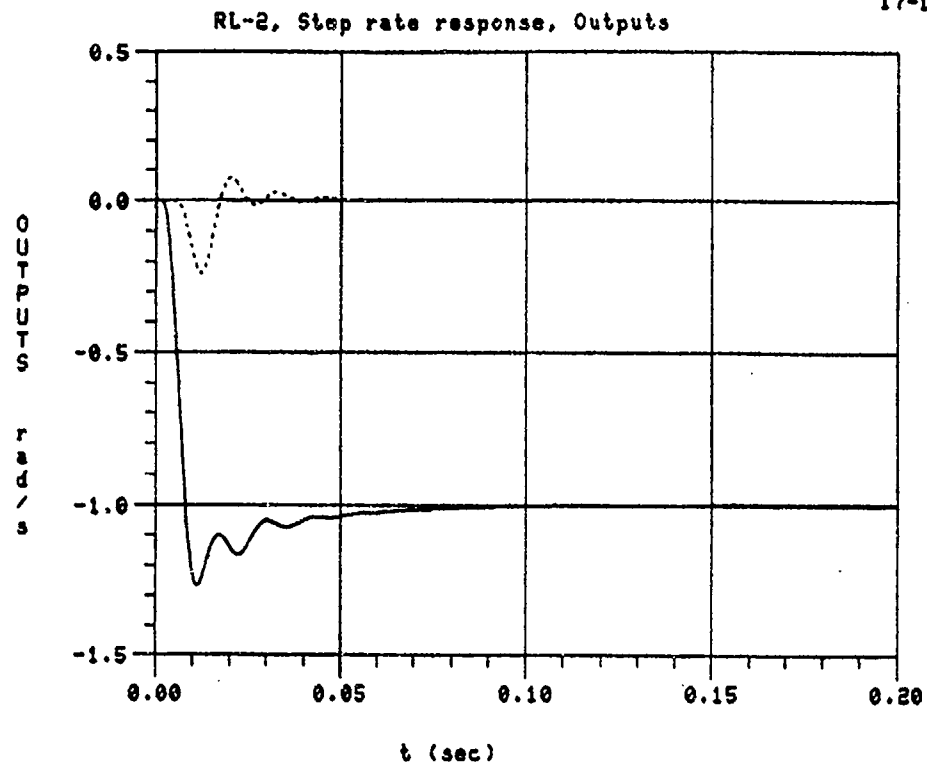
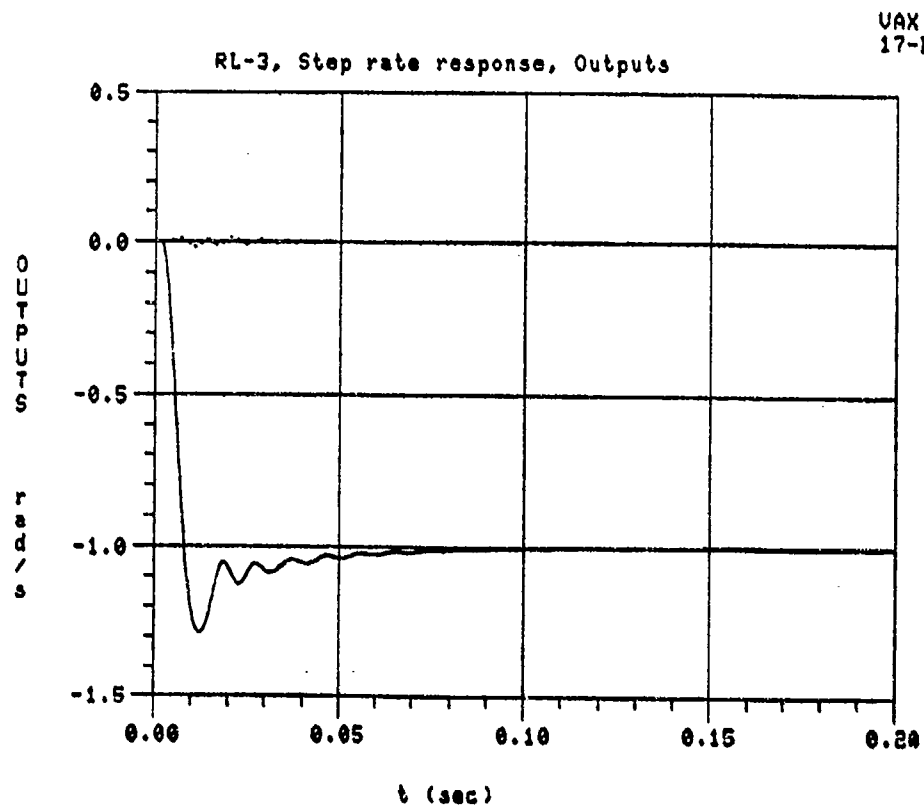
The system outputs, OUT_x and OUT_y , and the pickoffs, θ_x and θ_y , are examined for both RL-2 and RL-3 for step changes in case rate (0 to 1 rad/s at $t=0$) and acceleration (0 to 1 rad/s/s at $t=0$) on the x case input axis. The results are shown in Figures 4 through 8. First note that the transients are all practically negligible after about 0.1 seconds indicating a very tight loop that should meet the requirements for a strapdown gyro.

For a step rate case input, the direct outputs of each loop (Figure 4) exhibit an overshoot of about 30%, for a step

rate input, and some slight ringing for a few milliseconds which is quite acceptable. One of the principle differences between RL-2 and RL-3 can be seen from these same figures in their cross-axis transients. In RL-3 they are very much reduced from what is exhibited in RL-2. This is the effect of the "cross-axis compensation" that was designed into RL-3. (Analogous comments for the pickoffs, Figure 5.)

For a step change in acceleration, the results are shown in Figure 6. The direct-axis rate outputs blow up since they indicate the input case rate, a linearly increasing function. It is the cross-axis outputs that demonstrate the other major advantage of RL-3. The cross-axis responses are magnified in Figure 7 for effect. The y-output of RL-2 shows that a steady-state rate was applied to the y-input when in fact there was none. The magnitude of this "apparent" rate is equal to $1/\omega_n$ times the magnitude of the input acceleration on the other axis, where ω_n is the nutation frequency, 1036.7255 rad/s. In RL-3, this effect completely dies out after a few milliseconds (see Figure 7b and note the vertical scale is 10 times larger than that of Figure 7a). This is called "acceleration cancellation". The pickoff response to accelerations (Figure 8) of RL-2 and RL-3 is much the same, differing in the magnitude of the cross-axis transients. The x-pickoff exhibits the same steady-state value in both loops so the actual "cancellation" is done at the outputs, not the pickoffs. In the next section, the expected steady-state output and pickoff values are computed for different inputs to verify the simulations.

In summary, the time responses appear to be quite satisfactory for both loops, the major differences being the amount of cross-axis transient response (reduced by roughly a factor of 10 in RL-3) and the steady-state acceleration effect (the steady-state output on the y-axis for an acceleration of 1 rad/s/s on the x-axis is $-1/1036.7255 = -0.0009646$ rad/s for RL-2 but is zero for RL-3).

Fig. 4a: RL-2 step rate response (outputs); — OUT_x , --- OUT_y Fig. 4b: RL-3 step rate response (outputs); — OUT_x , --- OUT_y

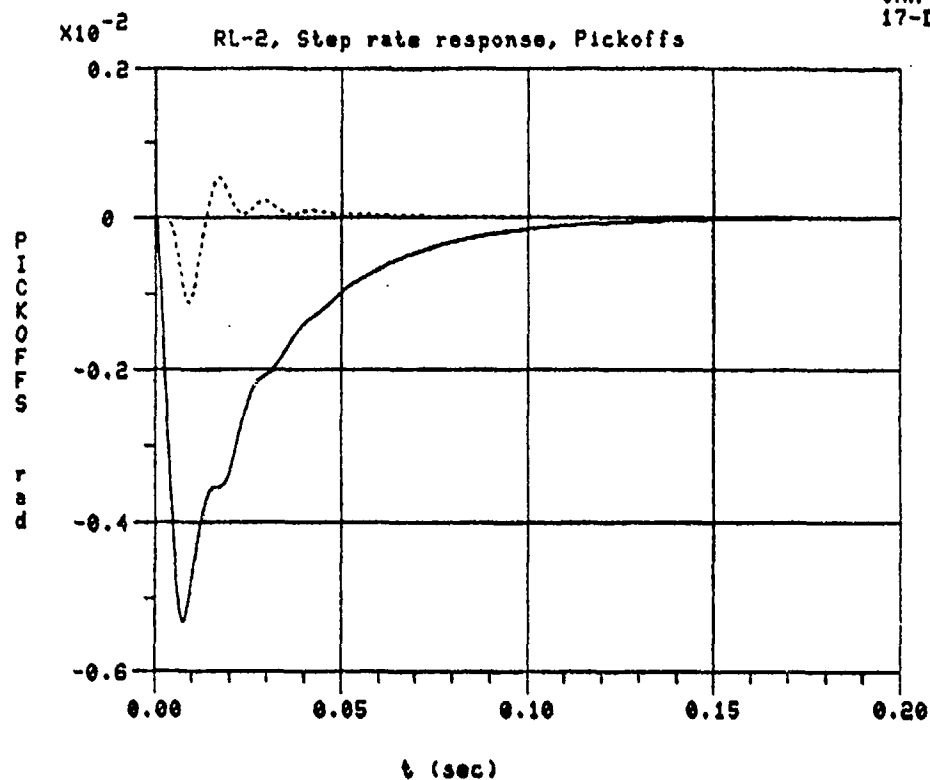


Fig. 5a: RL-2 step rate response (pickoffs); — θ_x , --- θ_y

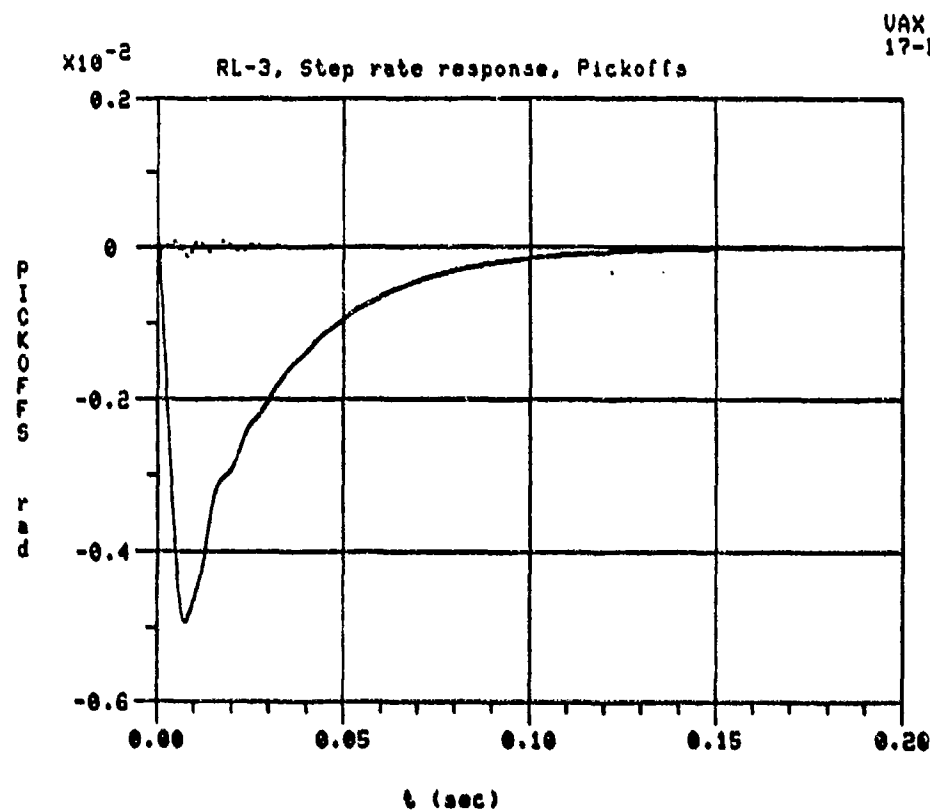
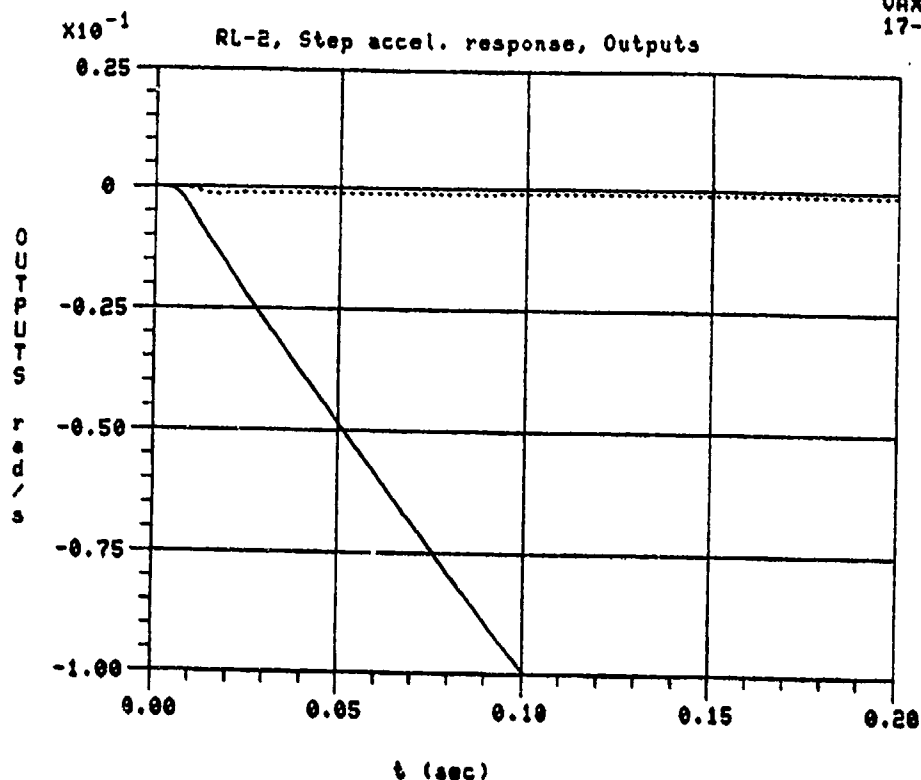
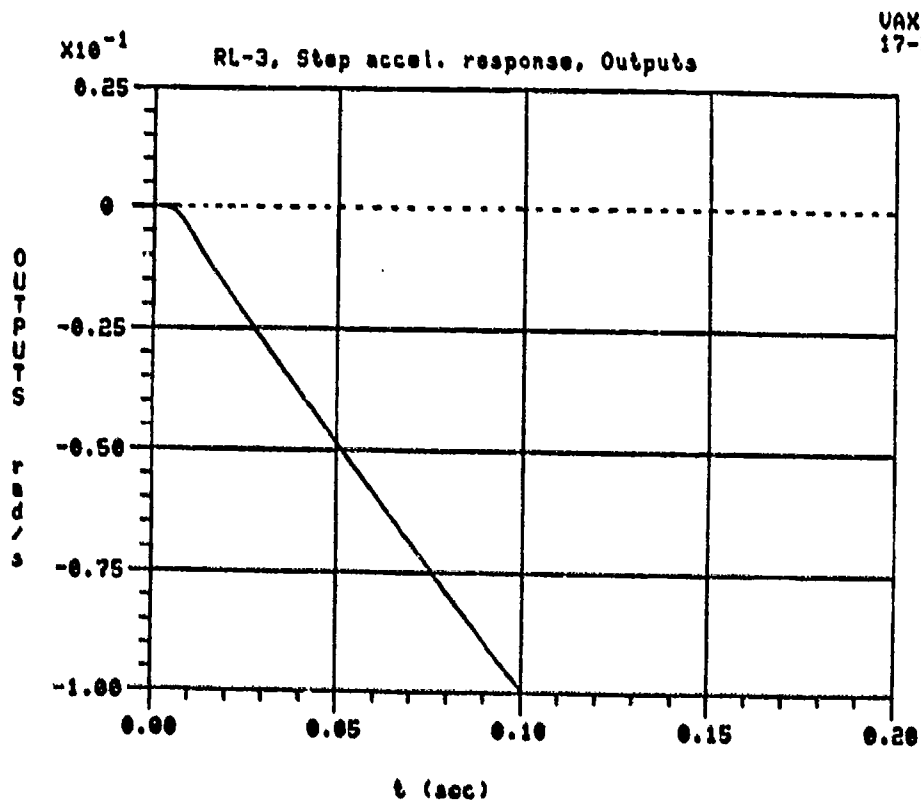


Fig. 5b: RL-3 step rate response (pickoffs); — θ_x , --- θ_y

Fig.6a: RL-2 step acceleration response (outputs); $-OUT_x$, $--OUT_y$ Fig.6b: RL-3 step acceleration response (outputs); $-OUT_x$, $--OUT_y$

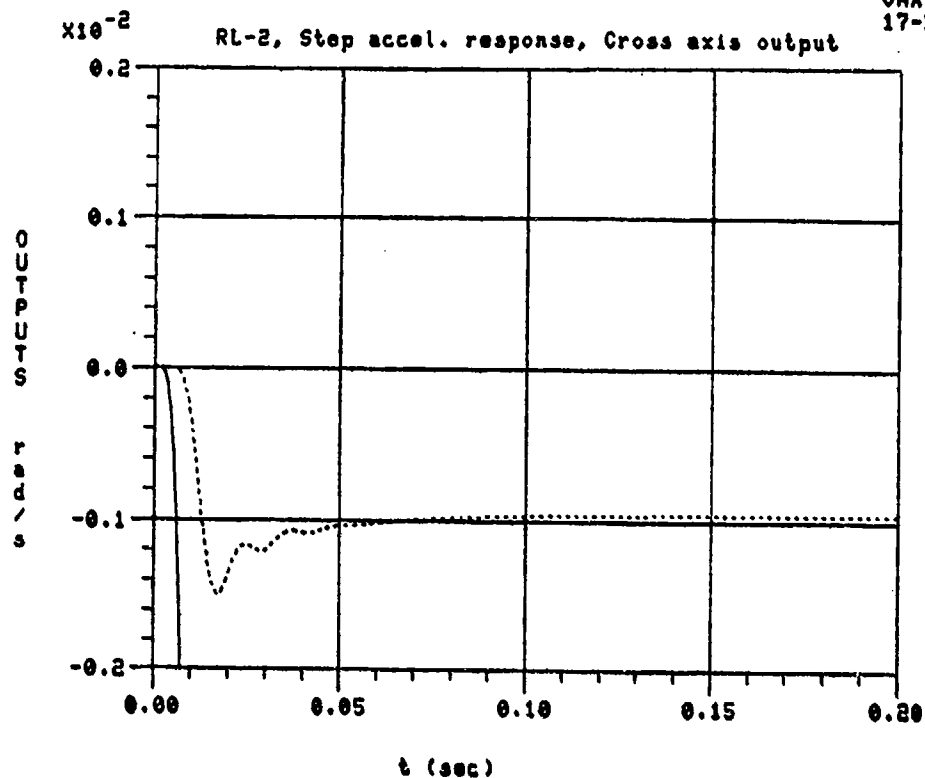


Fig. 7a: RL-2 step acceleration response (cross-axis); --- OUT_y

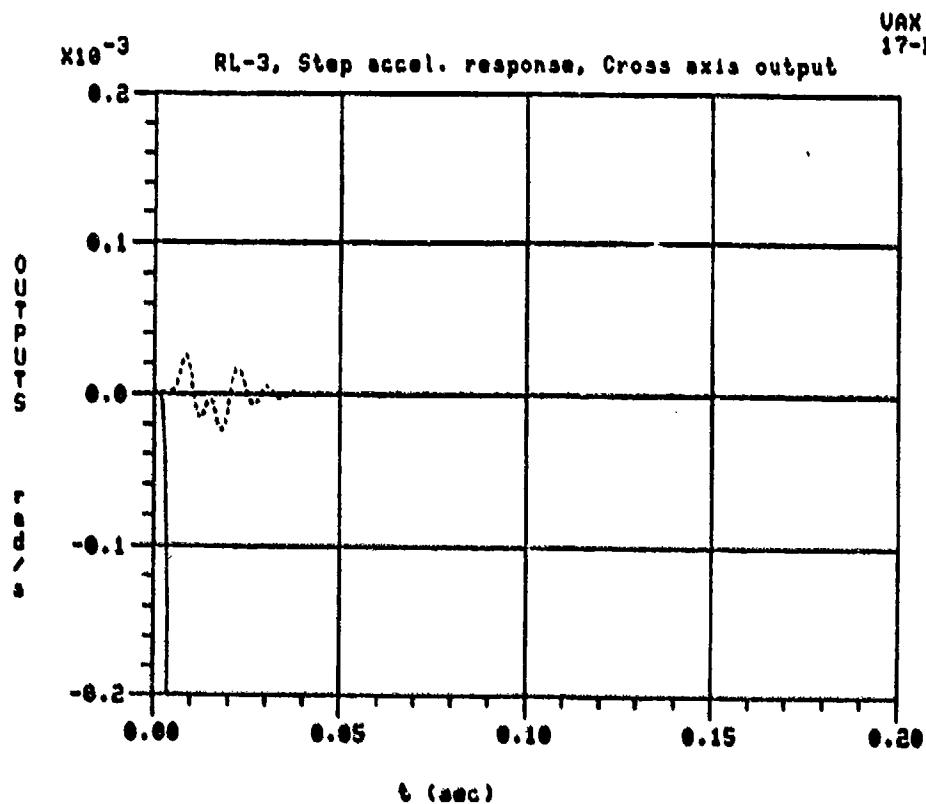
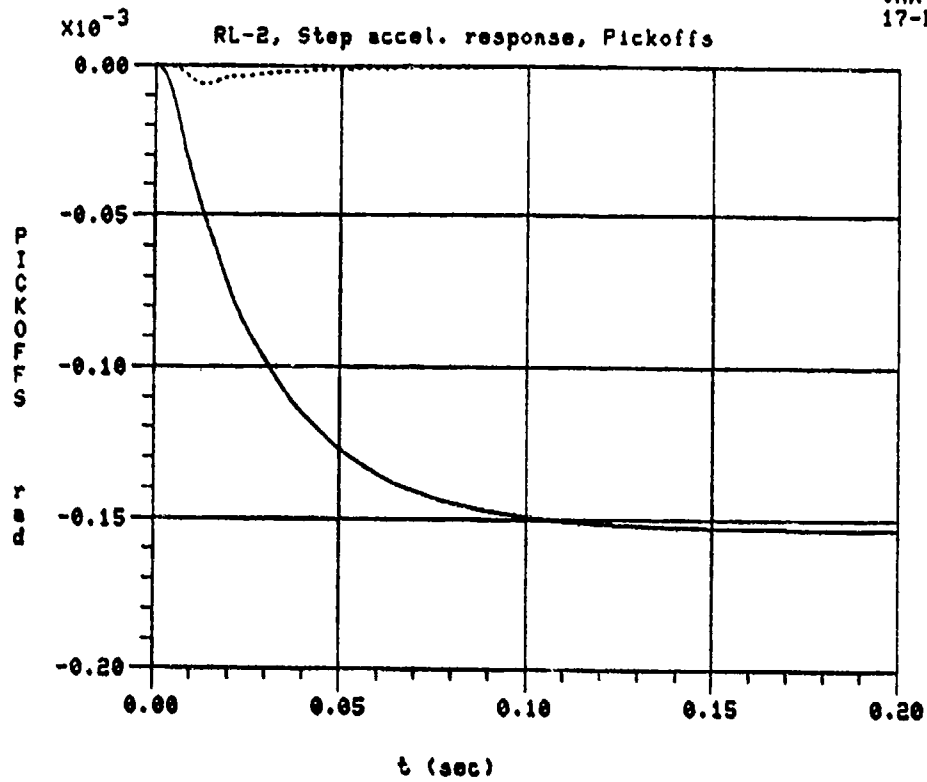
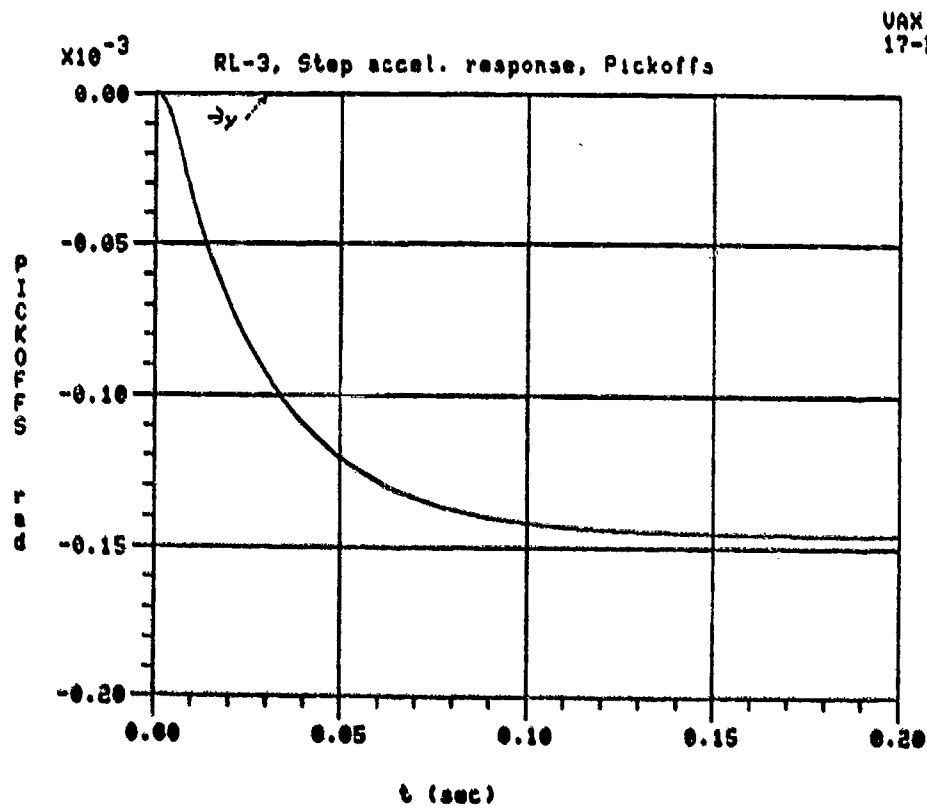


Fig. 7b: RL-3 step acceleration response (cross-axis); --- OUT_y

Fig. 8a: RL-2 step acceleration response (pickoffs); $-\theta_x$, $-\theta_y$ Fig. 8b: RL-3 step acceleration response (pickoffs); $-\theta_x$, $-\theta_y$

4.2.2 Steady-State Results

Steady-state responses to step changes of input rates and accelerations are computed with the frequency domain model and the final value theorem. Briefly, the final value theorem states that the steady-state time response, $g(t \rightarrow \infty)$, of a STABLE system, $L(s)$, to an input signal $f(s)$ can be found by

$$\lim_{t \rightarrow \infty} g(t) = \lim_{s \rightarrow 0} s L(s) f(s) .$$

The input signal will be taken as

$$\begin{bmatrix} \omega_{cx} \\ \omega_{cy} \end{bmatrix} = \begin{bmatrix} 1 \\ 0 \end{bmatrix} \frac{1}{s^n}$$

where $n=1$ for a constant rate on the x case axis and $n=2$ for a constant acceleration. The y input is fixed as 0. Since the closed-loop stability of both RL-2 and RL-3 has been established, it is valid to use the final value theorem. The steady-state outputs of the closed-loop system (6) are found by:

$$\begin{aligned} \lim_{t \rightarrow \infty} \begin{bmatrix} \text{OUT}_x(t) \\ \text{OUT}_y(t) \end{bmatrix} &= \lim_{s \rightarrow 0} s \begin{bmatrix} \text{OUT}_x(s) \\ \text{OUT}_y(s) \end{bmatrix} \\ &= \lim_{s \rightarrow 0} \frac{s}{s^n} \frac{-D}{(\tilde{s}^2 + C)^2 + (\tilde{s} + D)^2} \begin{bmatrix} \tilde{s}(\tilde{s}^2 + C + 1) + D & -D\tilde{s} + C \\ D\tilde{s} - C & \tilde{s}(\tilde{s}^2 + C + 1) + D \end{bmatrix} \begin{bmatrix} 1 \\ 0 \end{bmatrix} \end{aligned}$$

As an example, the final outputs of RL-3 under constant acceleration ($n=2$) on the x -axis are computed:

$$\lim_{t \rightarrow \infty} \begin{bmatrix} \text{OUT}_x(t) \\ \text{OUT}_y(t) \end{bmatrix} = \lim_{s \rightarrow 0} \frac{-D/s}{(\tilde{s}^2 + C)^2 + (\tilde{s} + D)^2} \begin{bmatrix} \tilde{s}(\tilde{s}^2 + C + 1) + D \\ D\tilde{s} - C \end{bmatrix}$$

$$\begin{aligned}
&= \lim_{s \rightarrow 0} \frac{-D}{D^2} \frac{-D/s}{\left(\frac{\tilde{s}^2+C}{D}\right)^2 + \left(\frac{\tilde{s}}{D} + 1\right)^2} \left[\frac{\tilde{s}(\tilde{s}^2+C+1)/D+1}{\tilde{s}-C/D} \right] \\
&= \lim_{s \rightarrow 0} - \left[\frac{\frac{\tilde{s}}{sD}(\tilde{s}^2+C+1) + \frac{1}{s}}{\frac{\tilde{s}}{s} - \frac{C}{Ds}} \right] \quad (10) \\
&= \lim_{s \rightarrow 0} - \left[\frac{\frac{1}{\omega_n D}(\tilde{s}^2+C+1) + \frac{1}{s}}{1/\omega_n - C/(Ds)} \right] .
\end{aligned}$$

The fact that $1/D(0) = 0$, due to the integrator, has been used to obtain (10). Now recall from the structure of $D(s)$ and $C(s)$ that $C(0) = (p_1)(p_2)(p_8)$ and note that the limit (as $s \rightarrow 0$) of $sD(s)$ is $(p_1)(p_2)$, so

$$\lim_{t \rightarrow \infty} \begin{bmatrix} \text{OUT}_x(t) \\ \text{OUT}_y(t) \end{bmatrix} = - \begin{bmatrix} 0 \\ 1/\omega_n - p_8 \end{bmatrix} .$$

With a choice of $p_8 = 1/\omega_n$, zero steady-state y output for an input x acceleration results. Of course, the x output has gone to negative infinity since the input x rate has gone to plus infinity.

Other outputs are computed similarly. The steady-state pickoffs can be found in this way too since, from (5),

$$\theta(s) = 1/[D(s)\omega_n] \text{OUT}(s).$$

The results are compiled in Table 3.

Table 3: Steady-state values

Input	RL-2				RL-3			
	Pickoffs		Outputs		Pickoffs		Outputs	
	θ_x	θ_y	OUT _x	OUT _y	θ_x	θ_y	OUT _x	OUT _y
$\omega_{cx} = k \text{ rad/s}$ (Rate)	0	0	-k	0	0	0	-k	0
$\omega_{cx} = k \text{ rad/s}^2$ (Acceleration)	$\frac{-k}{p_1 p_2 \omega_n}$	0	$-\infty$	$\frac{-k}{\omega_n}$	$\frac{-k}{p_1 p_2 \omega_n}$	0	$-\infty$	0 *

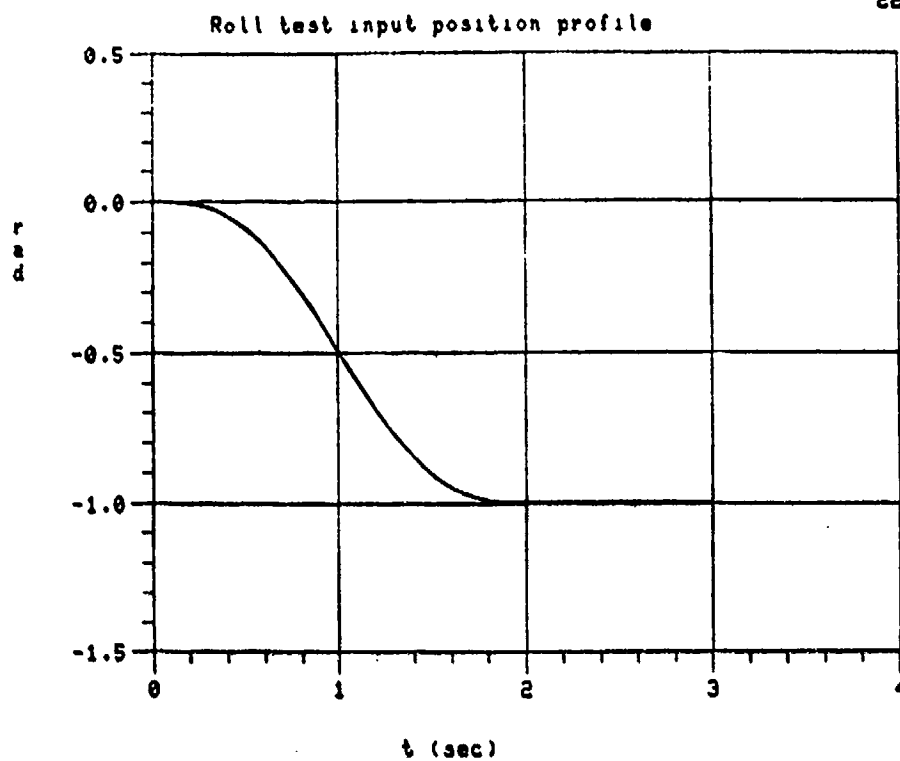
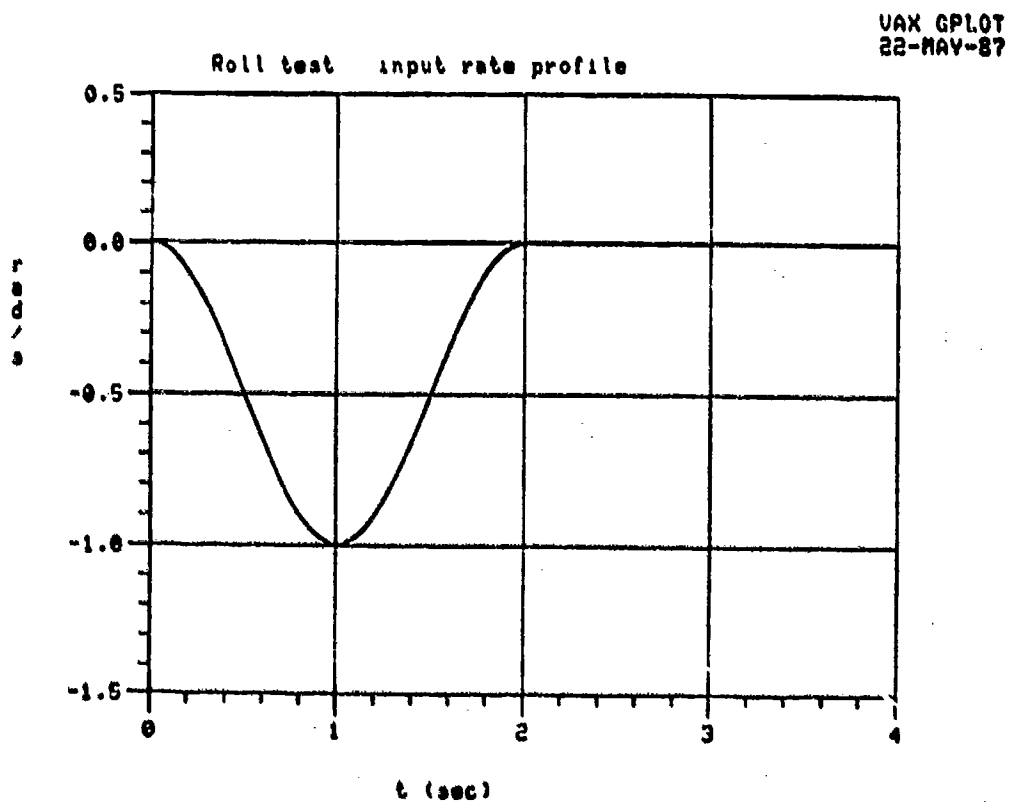
The steady-state results of RL-2 and RL-3 are identical except for the cross-axis output for constant acceleration. This is the acceleration cancellation that RL-3 provides. Note that, under constant acceleration, the x pickoff is nulled by neither loop; the acceleration cancellation is occurring at the outputs, not the pickoffs. Note also that this cancellation (the zero signified by * in the table) depends on p_g being exactly equal to $1/\omega_n$. Any deviation will result in a nonzero output. All the other zeros in the table have no such dependency. They were caused by multiplying a constant by an 's' and then letting s go to zero.

4.2.3 Roll Rate Tests

This brief section demonstrates that the rebalance loop causes no angular position error build-up as the gyro swings through an orientation change. A very simple model of an angular position profile of an aircraft roll is shown in Figure 9. This is made up of the following functions:

$$\phi_{cx}(t) = \begin{cases} 0.5t - \frac{0.5}{\pi} \sin \pi t, & 0 \leq t \leq 2 \\ 1.0, & 2 \leq t \end{cases}$$

This would correspond to an aircraft banking smoothly to a 1

Fig. 9: Roll test, input position profile = $-\phi_{cx}$ Fig. 10: Roll test, input rate profile = $-\dot{\omega}_{cx}$

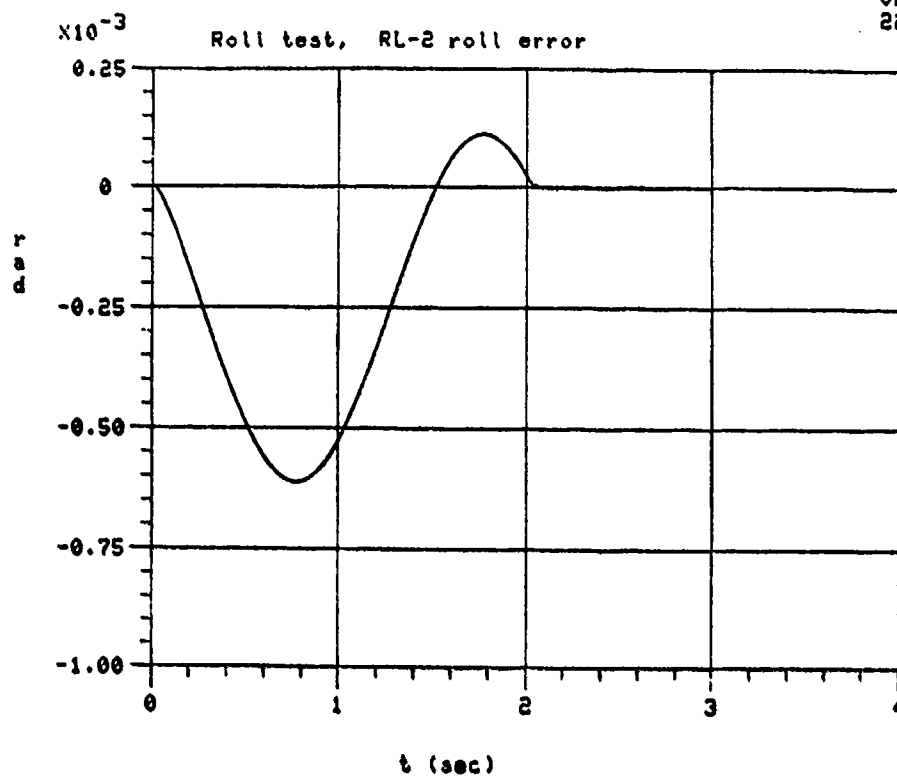


Fig. 11a: RL-2 roll error = $-\phi_{cx} - \int \text{OUT}_x$

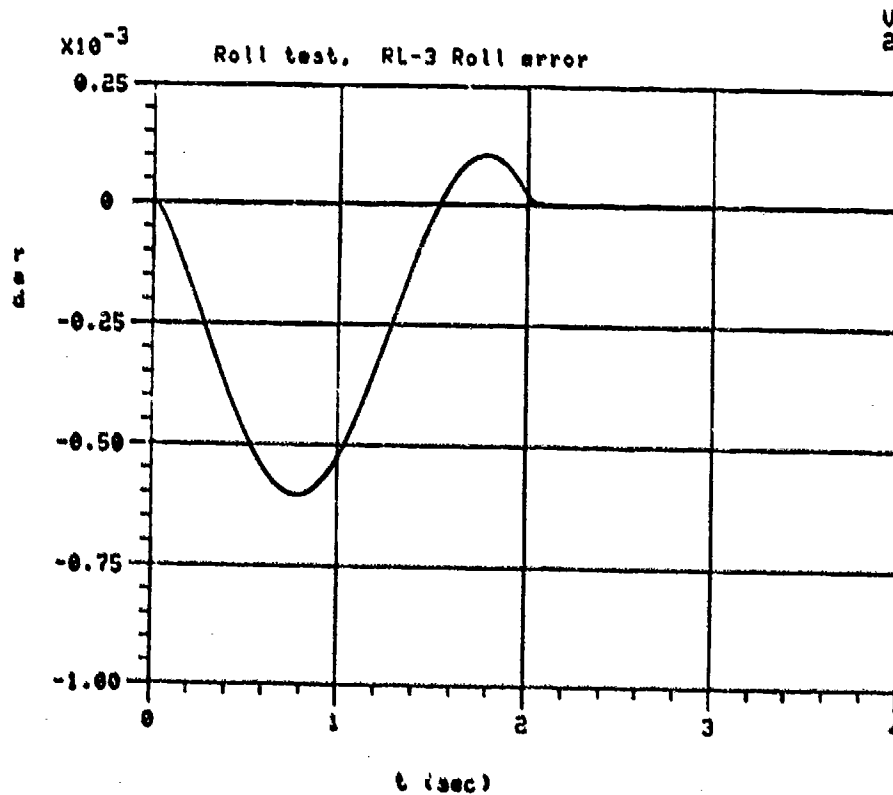
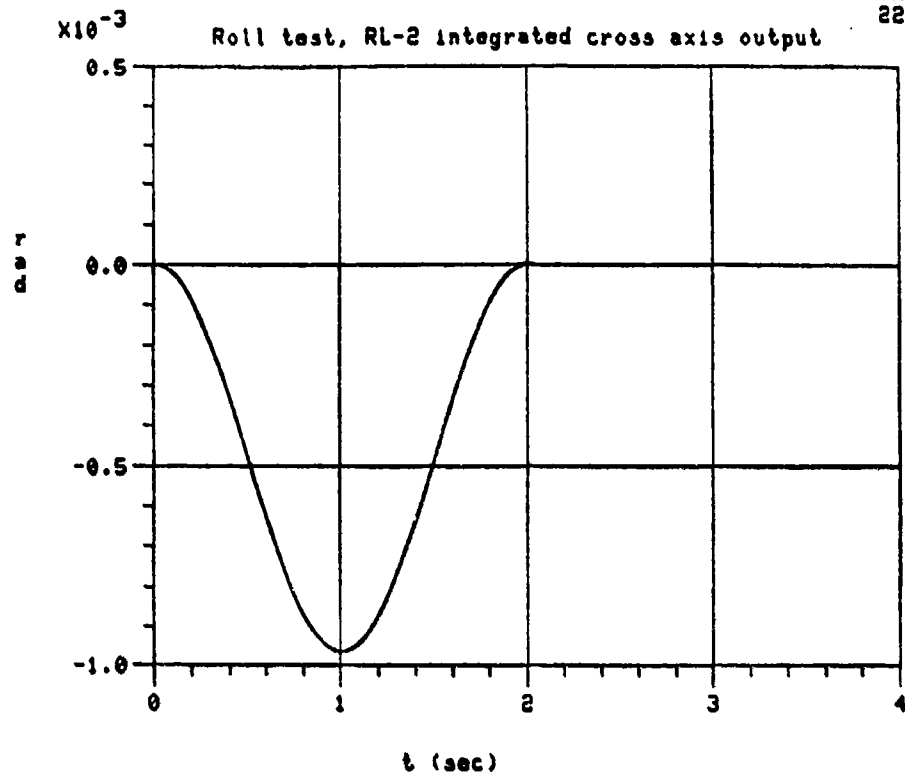
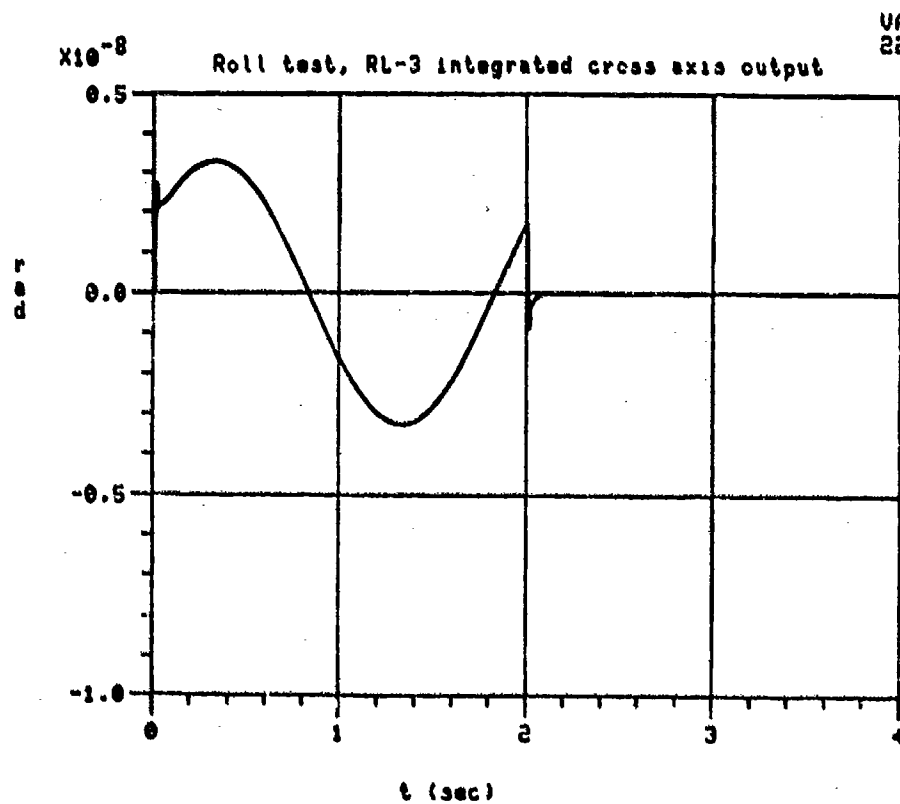


Fig. 11b: RL-3 roll error = $-\phi_{cx} - \int \text{OUT}_x$

Fig. 12a: RL-2 roll test, integrated cross-axis output = $\int \text{OUT}_y$ Fig. 12b: RL-3 roll test, integrated cross-axis output = $\int \text{OUT}_y$

radian (57 degree) roll angle in two seconds. The sinusoidal form is chosen as it appears realistic and it has continuous derivatives. Thus, the corresponding rates and accelerations are smooth as well. The input case rate profile, then, is

$$\omega_{cx}(t) = \begin{cases} 0.5 - 0.5 \cos \pi t, & 0 \leq t \leq 2 \\ 0. , & 2 \leq t \end{cases}$$

and is shown in Figure 10. The output rate and integrated output rate for both RL-2 and RL-3 trace the same curves as their corresponding inputs at these scales. Figure 11 shows the difference between the input angular position and the integrated output rate, which is called the roll error. It can be seen that during the maneuver, the roll error peaks at about 0.0006 rad (0.034 deg) for both RL-2 and RL-3 and returns to zero after the maneuver is completed. The impact of this error on navigation system accuracy will be minimal. For completeness, the integrated cross-axis outputs are shown in Figure 12. Note that the RL-3 response has been magnified 100,000 times, once again showing the superior cross-axis compensation of RL-3 for low frequency inputs.

4.3 Frequency Domain Characteristics

4.3.1 Closed-Loop Frequency Response

The closed-loop frequency response of equation (6) is repeated from [3]. The magnitude and phase responses of the direct and cross-axis closed loops for both RL-2 and RL-3 are shown in Figure 13. (The direct closed-loop shown here is the 1,1 element of the closed-loop transfer matrix which is identical to the 2,2 element. The cross loop shown is the 2,1 element; the 1,2 element is identical but for an additional

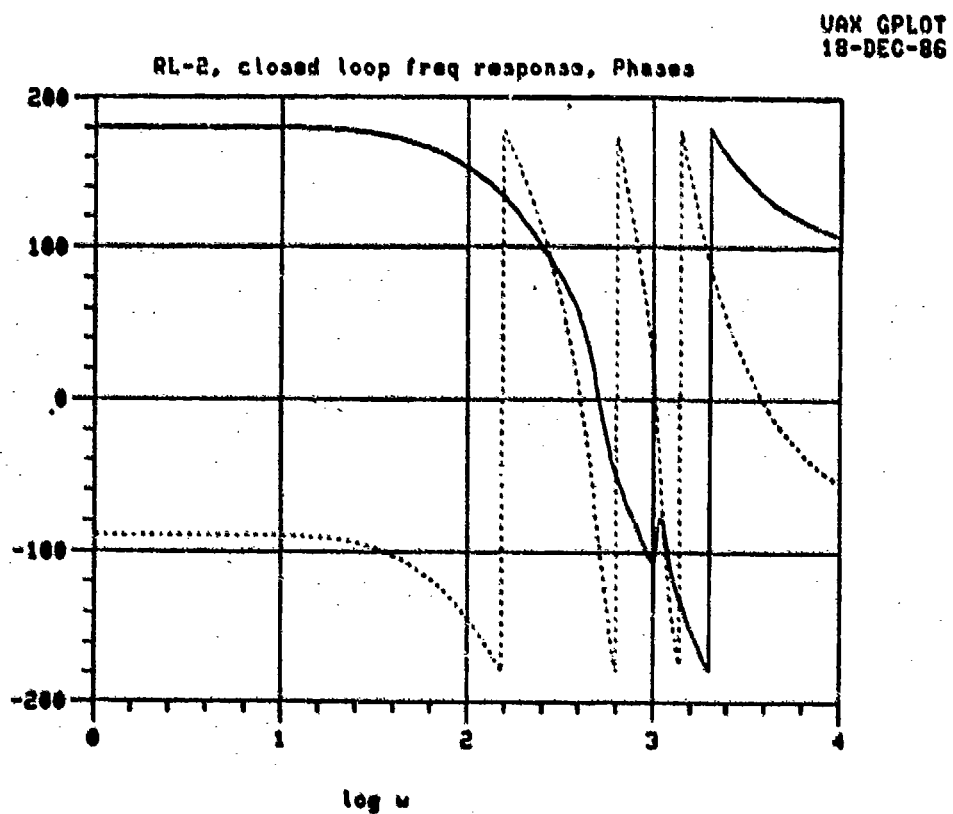
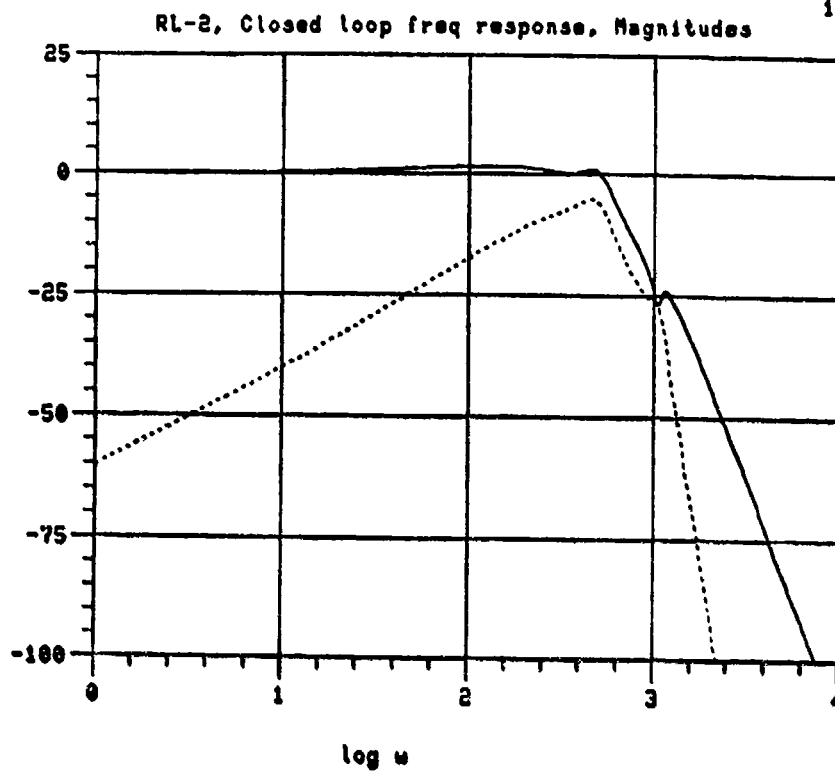
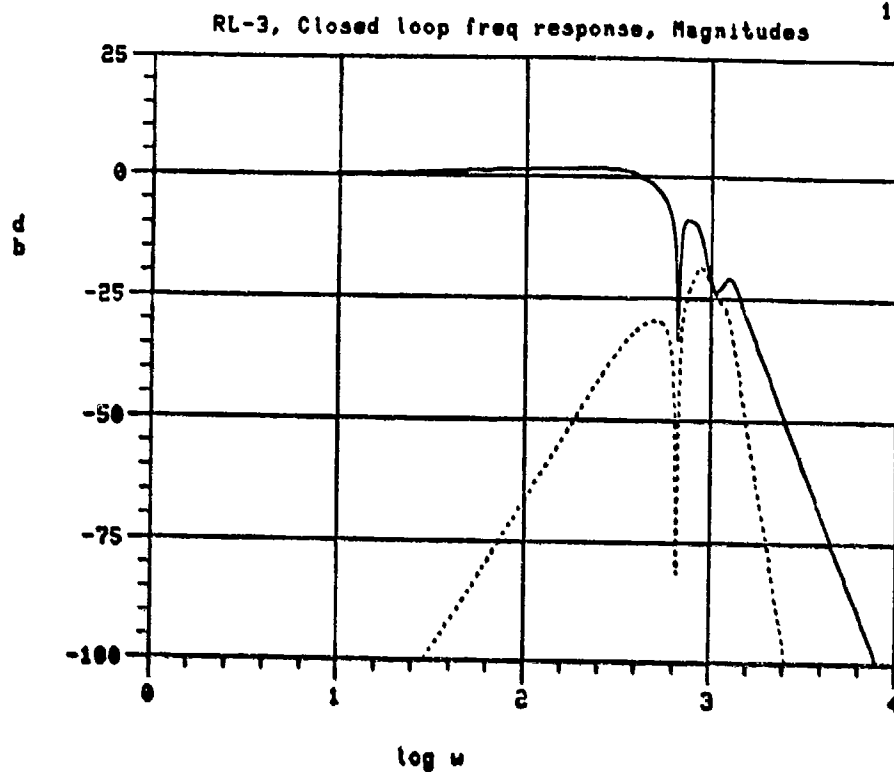


Fig.13a: RL-2 closed-loop frequency response, magnitude & phase
(— Direct axis, --- Cross axis)

VAX GLOT
18-DEC-86



VAX GLOT
18-DEC-86

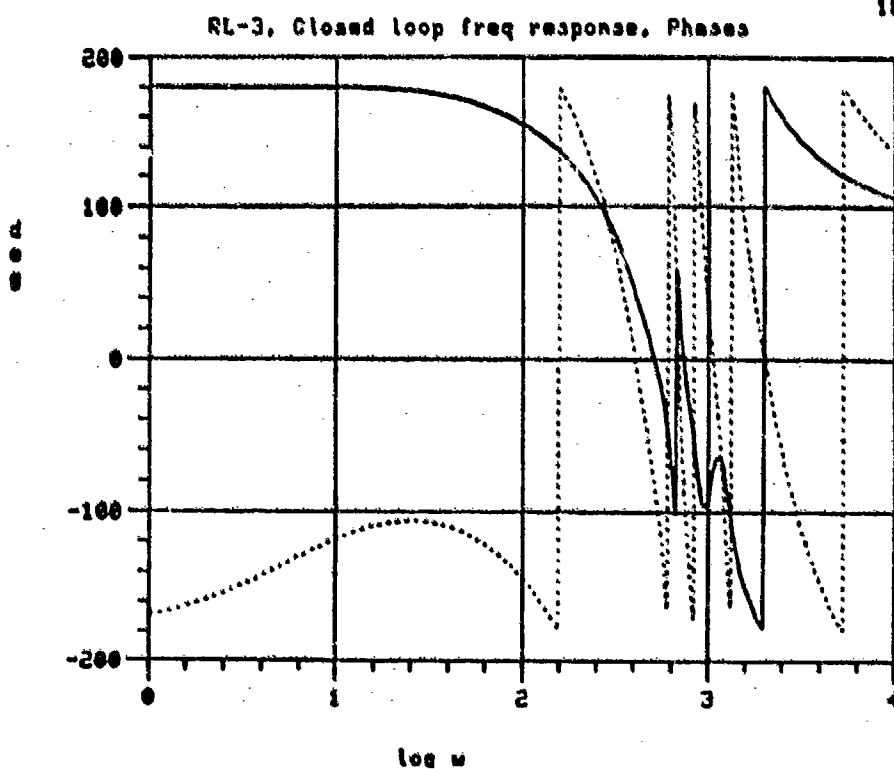


Fig.13b: RL-3 closed-loop frequency response, magnitude & phase
(— Direct axis, --- Cross axis)

phase shift of 180 degrees.)

Extensive interpretations of these are available in [3] so only a few comments are made. First, the horizontal scale of all frequency response plots is in terms of the log (base 10) of the radian frequency. The nutation frequency, for example, is at $\log_{10}(1036.7255)=3.016$. The bandwidth of the direct loop is around 80 Hz (2.70) for RL-3 and 90 Hz (2.75) for RL-2. Bandwidth here is defined as the frequency at which the magnitude drops to -3 db. The magnitude of the cross-axis transfer function is generally much larger for RL-2 than for RL-3. This is expected because the cross-axis compensator was designed specifically to reduce the magnitude of the cross-axis transfer function at low frequencies while leaving the high frequency response alone to provide for a stability margin. The deep notch in the magnitude function of RL-3 around 105.5 Hz (2.82 on the log scale) is due to the spin notch filter in the direct-axis.

4.3.2 The Sensitivity Function

A very powerful frequency domain tool to analyze control systems is the sensitivity function. It provides at least two valuable pieces of information. It gives an indication of, first, how well the closed-loop system "tracks" its inputs, and second, how "sensitive" the closed-loop system is to changes in the open-loop.

Consider the system of Figure 1 as though it were a single-loop system, with open-loop transfer function $P(s)K(s)$ and closed-loop function $\phi_r(s) = M(s)\phi_c(s)$, $M(s) := -P(s)K(s)/(1-P(s)K(s))$. The sensitivity function, $S(s)$, is defined by

$$S(s) := \frac{\partial M/M}{\partial (PK)/(PK)} = \frac{1}{1-PK}.$$

For multivariable systems the open-loop is a matrix $P(s)K(s)$ and the closed-loop matrix, from (4), is (dropping the s)

$\phi_r = M\phi_c$, $M = -PK[I-PK]^{-1}$. Though the mechanics of derivatives with respect to matrices is more involved, the end result is the definition of the multivariable (output) sensitivity function,

$$S(s) := [I-PK]^{-1}$$

analogous to the single-loop case. But this function is exactly the function in equation (4) relating the pickoff angle, θ , to the input case angle, ϕ_c . Therefore if the magnitude of the sensitivity function is kept small over certain frequency ranges, then the magnitude of the pickoff angle (the tracking error) will be small for input angular positions at those frequencies, since $|\theta(j\omega)| \leq |S(j\omega)| |\phi_c(j\omega)|$.

The obvious question is how to measure the magnitude of a matrix. The simplest way, since this system is only a 2 by 2 system that is in fact nearly symmetric (with equal diagonal terms and only the signs of the off-diagonal elements differing), is to look at the magnitudes of individual elements to get direct and cross-axis sensitivity functions. This is done in Figure 14 where the magnitudes of the direct and cross-axis sensitivity functions are plotted as functions of frequency for both RL-2 and RL-3.

The direct-axis sensitivity functions tend toward 0 ($-\infty$ db) at zero frequency ($-\infty$ on the log scale) indicating zero asymptotic tracking error of constant angular position inputs; furthermore their slopes, as the frequency approaches zero, are 40 db/decade indicating that constant rate inputs are asymptotically tracked as well (a 20 db/decade slope indicates a $1/s$ in the loop to null angular position errors, a 40 db/decade slope indicates a $1/s^2$ in the loop to null rate errors as well); their magnitudes are below -20db (.1 gain) for frequencies up to approximately 30 rad/s or 5 Hz (1.5 on log scale) which is very good low frequency tracking (the same can be seen from the closed-loop frequency response; the magnitude response is flat well beyond 5 Hz but the phase starts to drop appreciably above 5 Hz creating sinusoidal

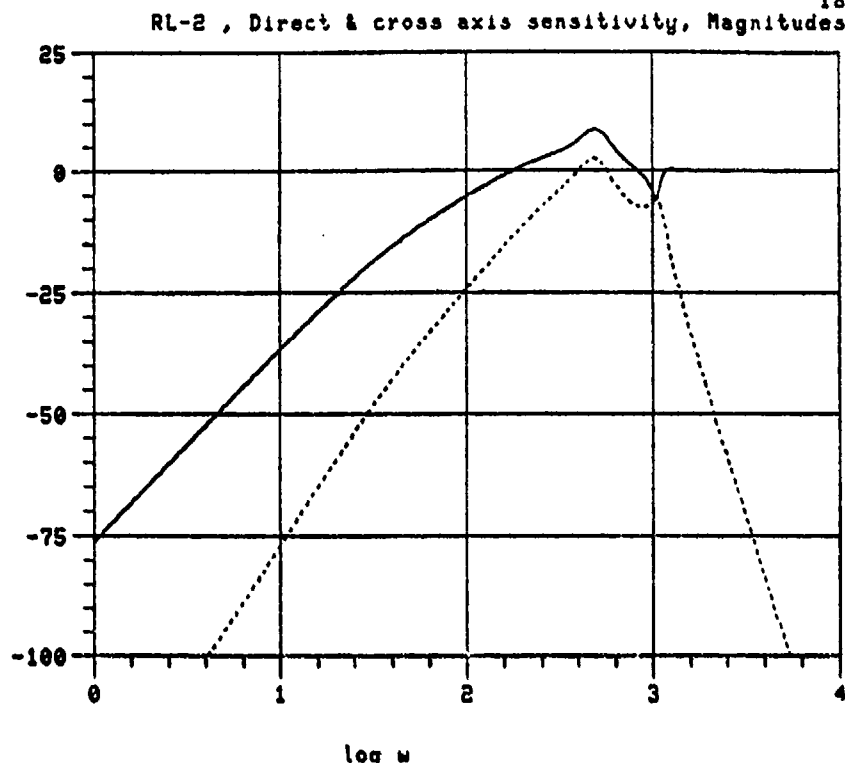
UAX GPLOT
18-DEC-86

Fig. 14a: RL-2 sensitivity functions; — Direct, --- Cross

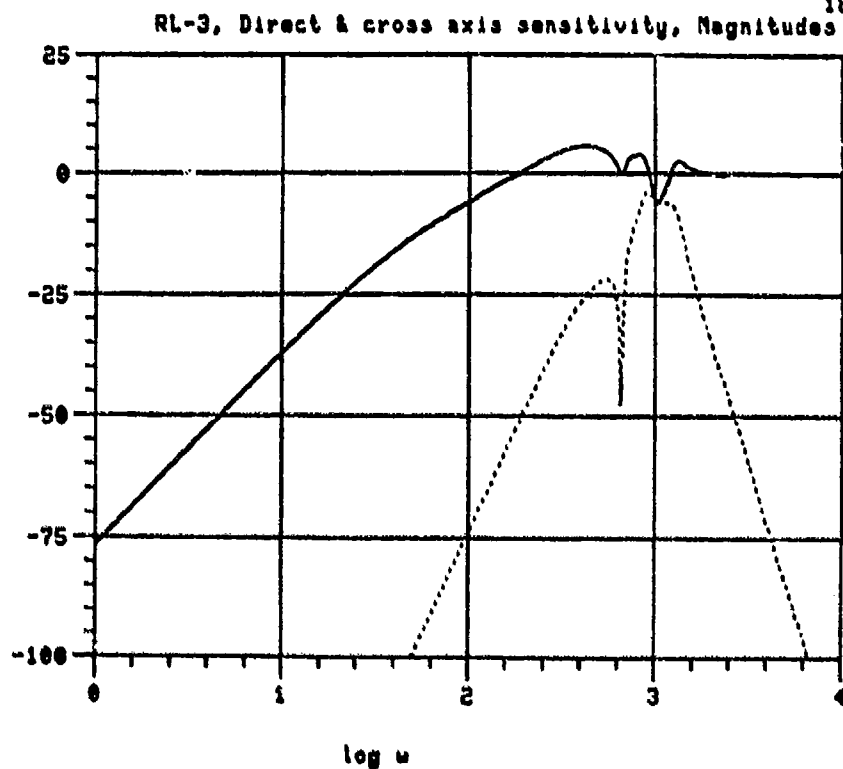
UAX GPLOT
18-DEC-86

Fig. 14b: RL-3 sensitivity functions; — Direct, --- Cross

steady-state tracking errors); the sensitivity is greater than 0 db for frequencies above 180 rad/s or 30 Hz (2.25 on the log scale) indicating poor tracking of these frequencies. It is noted that RL-3 has a little better direct-axis sensitivity than RL-2 as it has a lower peak (6 db compared to 10 db).

The sensitivity in the frequency range from 30 to 80 Hz (2.25 to 2.7) may be of some concern to the behavior of the system, as this range is essentially within the closed-loop bandwidth. Should there be any significant open loop uncertainties in this range, the closed-loop response may not be as expected since the system is fairly sensitive at these frequencies. At lower frequencies the sensitivity is significantly less and at higher frequencies, the closed-loop bandwidth is exceeded so any effects would be attenuated. This frequency range is typically outside most vehicle maneuver capabilities and would only be of concern in a high vibration environment and when there is significant uncertainty in the models.

Similar remarks can be made about the cross-axis sensitivity function. The cross-axis sensitivity of RL-3 is much lower, over the bandwidth, than that of RL-2. Again this is one of the intentions of RL-3 - to reduce the magnitude and the sensitivity of the cross-axis.

A more mathematically precise way to measure the size of a matrix is through the use of a suitable norm such as the matrix 2-norm. The 2-norm of a complex-valued matrix $S(j\omega)$ is the square root of the maximum eigenvalue of $S^*(j\omega)S(j\omega)$ where $S^*(j\omega)$ denotes the complex conjugate transpose of $S(j\omega)$. This quantity is known as the maximum singular value of $S(j\omega)$ and so the norm is often referred to as the singular value norm. In Figure 15 the maximum singular values of the sensitivity functions of RL-2 and RL-3 are plotted as functions of frequency. These plots indicate essentially the same things as the direct-axis sensitivity functions so they are discussed no further. There is a partially developed theory to ensure the

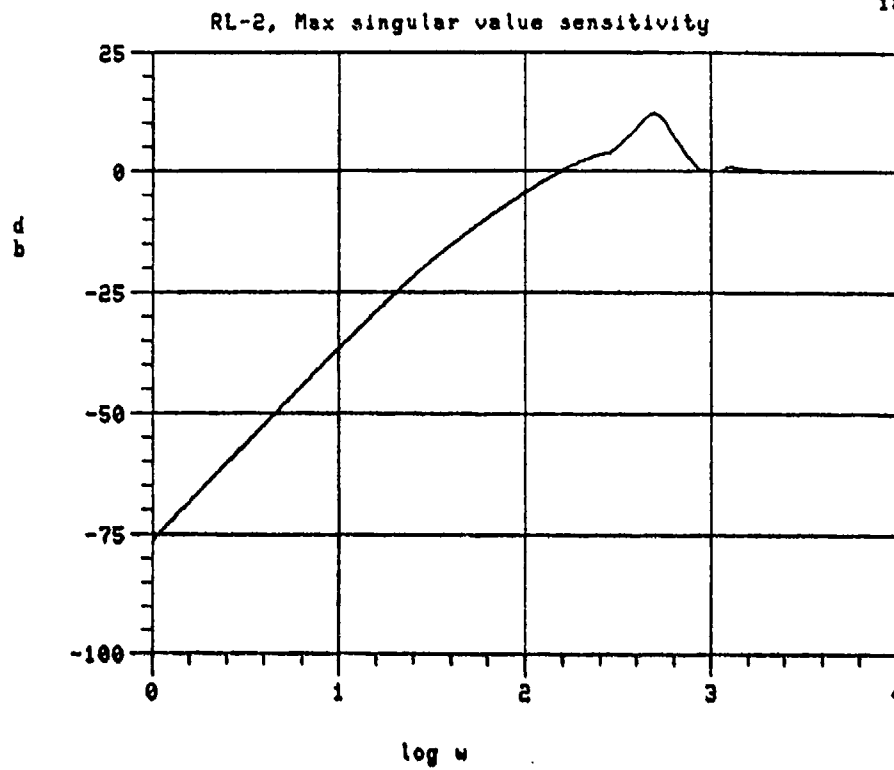


Fig. 15a: RL-2 maximum singular value sensitivity function

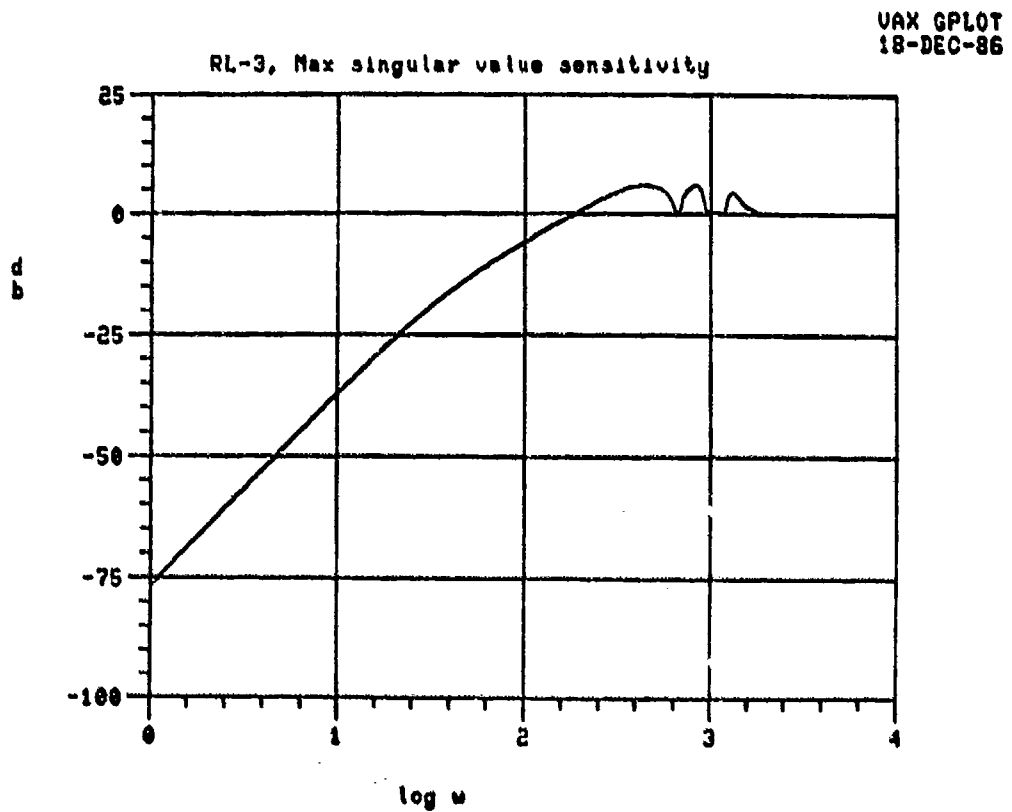


Fig. 15b: RL-3 maximum singular value sensitivity function

robust stability of a closed-loop system under certain plant changes based on this singular value norm. The approach was applied to this problem but the results were inconclusive for a number of reasons, so the procedure was dropped.

In summary, the sensitivity functions of both loops appear well behaved both in terms of tracking and parameter sensitivity.

4.3.3 Nyquist Plots

The Nyquist plot, one of the most important tools for the design and analysis of single-loop systems, carries over logically to multivariable systems but its interpretation does not. Two types of Nyquist plots were used. The first was the well known multivariable form, i.e., the image of the Nyquist "D-contour" under the map $\det[I-PK]$, where "det" signifies determinant, must satisfy certain encirclement criteria. For the second type, one of the loops on one axis of the gyro was broken and the resulting system was considered as single-input, single-output.

For single-loop systems, the Nyquist criterion is well known: the image of the standard D-contour under the map, $1+L(s)$, where $L(s)$ is the open-loop transfer function, must encircle the origin as many times as there are unstable poles of $L(s)$. Typically, one looks at the image under the map $L(s)$ and checks for encirclements of the $(-1+j0)$ point which is equivalent. For rigorous definitions of D-contour and encirclements, see any text on classical control. If the system is open-loop stable, the gain and phase margins are read directly off the Nyquist plot.

For multivariable systems, the criterion is that the image of the map $\det[I+L(s)]$ must encircle the origin as many times as there are unstable poles of $L(s)$, counted according to McMillan degree (see [7], for example). However, it is not equivalent to plot the image of $\det[L(s)]$ and check the $(-1,0)$

point because of the determinant function. The loop transfer function for this problem is $L(s) = -P(s)K(s)$ which is marginally stable. It has 2 poles at the origin, due to the integrators in $K(s)$, and a pole at each of $+j\omega_n$ and $-j\omega_n$, due to the simple model of the gyro adopted. These poles are avoided when forming the D-contour as shown in Figure 16.

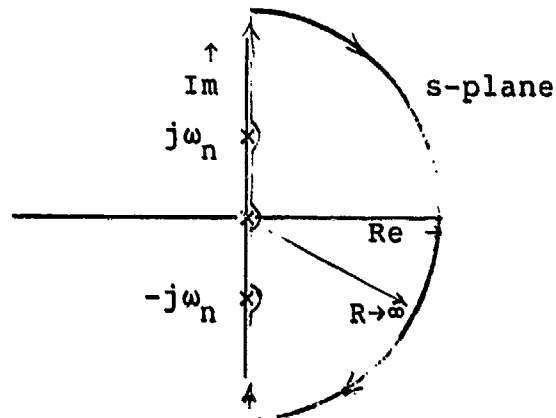


Fig. 16: Nyquist "D-contour"

The multivariable Nyquist plots of both RL-2 and RL-3 were computed and plotted but were found to be very complicated. There were several circles of infinite radius due to the small indentations around the open-loop poles on the imaginary axis. It was found, by tracing the curves carefully, that there was one clockwise and one counterclockwise encirclement of the origin for a net of zero encirclements which equals the number of open-loop poles in the right half plane. This verified that the closed-loop was indeed stable but there was no direct indication of a measure of gain or phase margin available from it. The reason for this is the complex way in which the determinant function intertwines the four transfer functions in the matrix $I - P(s)K(s)$. It was evident that there was some stability margin because the multivariable Nyquist plot did not go through the origin which would have indicated no margin.

For the second form of the Nyquist plot, one of the pickoff lines is opened while the other remains closed. In this sense, the remaining system can be interpreted as single-input - single-output and the traditional Nyquist criterion can be applied. With the system as shown in Figure 17 (with the x pickoff line broken), the following relations between a signal f injected at the loop breaking point and the resulting signal g at the plant output can be written:

$$\begin{bmatrix} g \\ \phi_{ry} \end{bmatrix} = -PK \begin{bmatrix} f \\ -\phi_{ry} \end{bmatrix} .$$

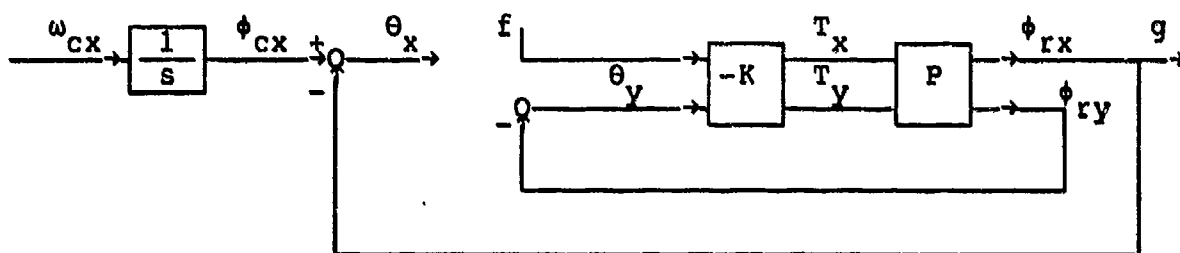


Fig. 17: System with one loop open

Upon substitution of the expressions of the plant and compensator matrices and simplification, the following transfer function results:

$$g(s) = L_o(s)f(s)$$

$$L_o(s) := \frac{\tilde{s}(C\tilde{s}+D) + C^2 + D^2}{\tilde{s}(\tilde{s}^3 + \tilde{s} + C\tilde{s} + D)} .$$

The function $L_o(s)$ will be called an "open-loop transfer function" though it is, in fact, a result of a system that is "half open" and "half closed". The image of the D-contour under $L_o(s)$ is then checked for encirclements of the (1,0) point.

Because of the "half open" structure, the Nyquist diagrams will need special interpretation.

The new "open-loop" function has no right half plane poles and it has only one imaginary axis pole, that being at the origin due to the integrator in the unclosed portion of the compensator. Then the Nyquist D-contour need only have one indentation along the imaginary axis (at the origin). The full Nyquist plot is then not necessary. It is sufficient to compute the portion of the Nyquist plot due to the positive imaginary axis (also called a polar plot) and ensure that it does not enclose the $(-1,0)$ point.

The new Nyquist plots for RL-2 and RL-3 are shown in Figure 18. Neither encloses the $(-1,0)$ point since they both cross the real axis to the right of $(-1,0)$, so closed-loop stability is once again verified. Now however, they look significantly more like classical Nyquist plots with somewhat more reasonable notions of gain/phase margins.

The gain margin (how much pure gain can be added to the open-loop before the closed-loop goes unstable) is directly available from classical Nyquist plots by simply determining how large the plot can be expanded before it goes through the critical $(-1,0)$ point. (Multiplying the open-loop by a pure gain will just expand the real and imaginary parts of the classical Nyquist plot equally; the shape will not change.) Similarly the phase margin is determined by how large an angle the plot can be rotated through before it goes through $(-1,0)$. Typical margins that classical designers try to achieve are 6 db gain margin and 60 degree phase margin.

The interpretations in this case are not quite so clear but the following measure is proposed: break one of the pickoff lines as above; to check the gain margin, replace the compensator matrix, $K(s)$, by $aK(s)$, where 'a' is a positive number, and increase 'a' until the Nyquist plot goes through $(-1,0)$; to find the phase margin, replace $K(s)$ by $e^{-jb}K(s)$,

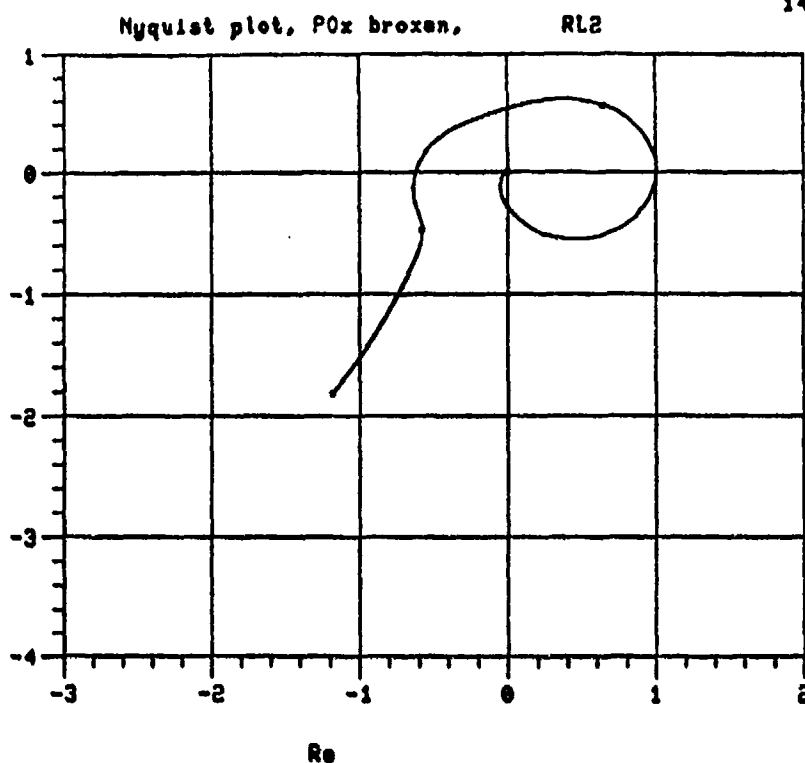


Fig. 18a: RL-2 Nyquist plot

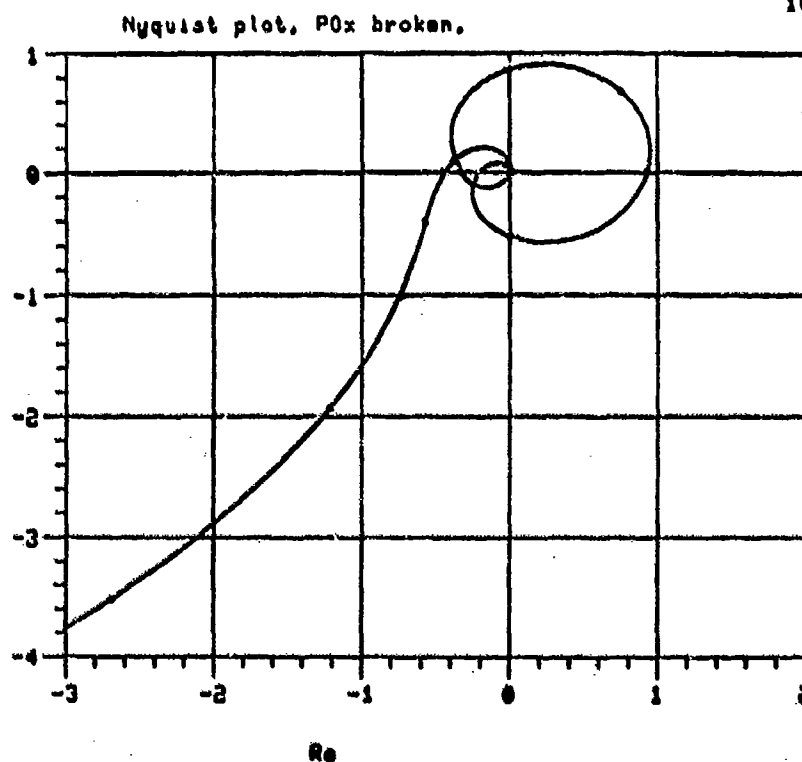
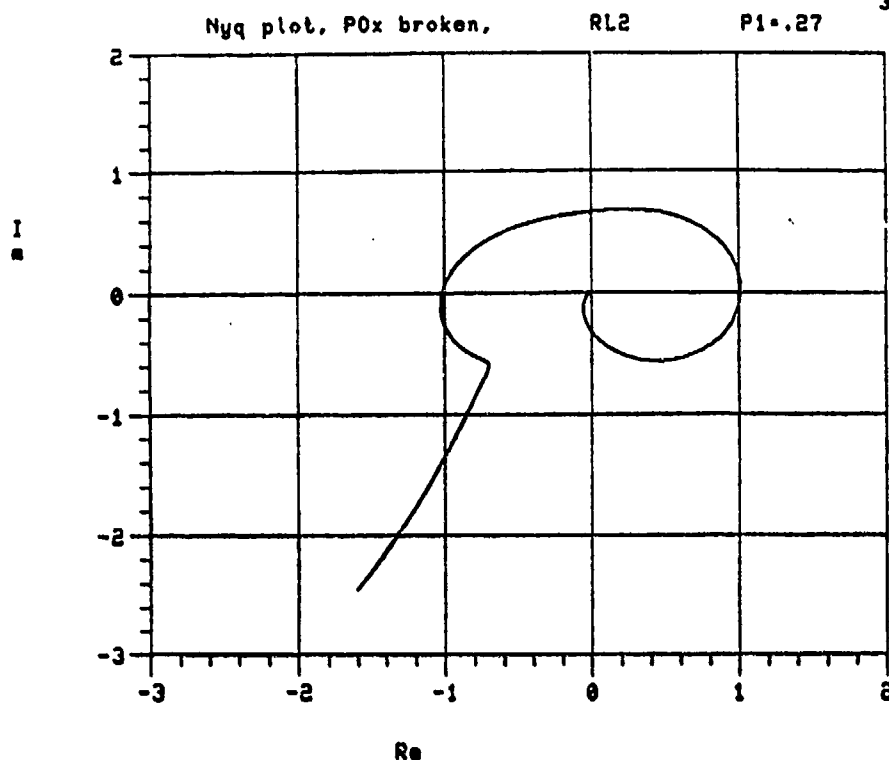
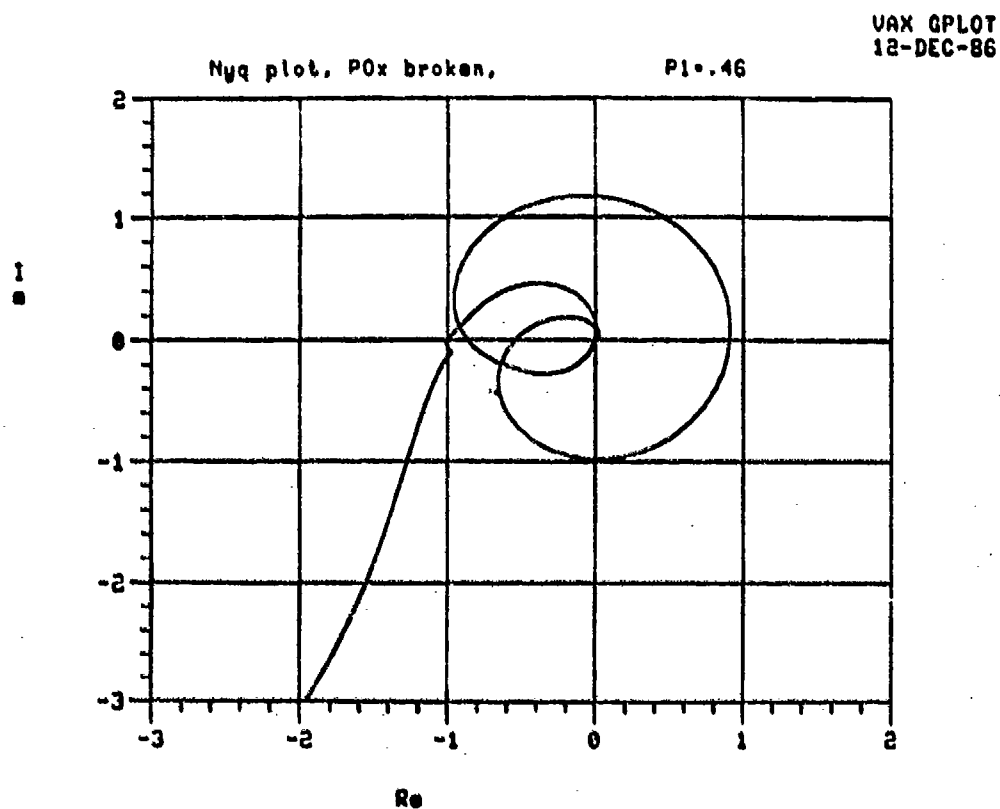


Fig. 18b: RL-3 Nyquist plot

Fig. 19a: RL-2 Nyquist plot, gain increased to $p_1=.27$ Fig. 19b: RL-3 Nyquist plot, gain increased to $p_1=.46$

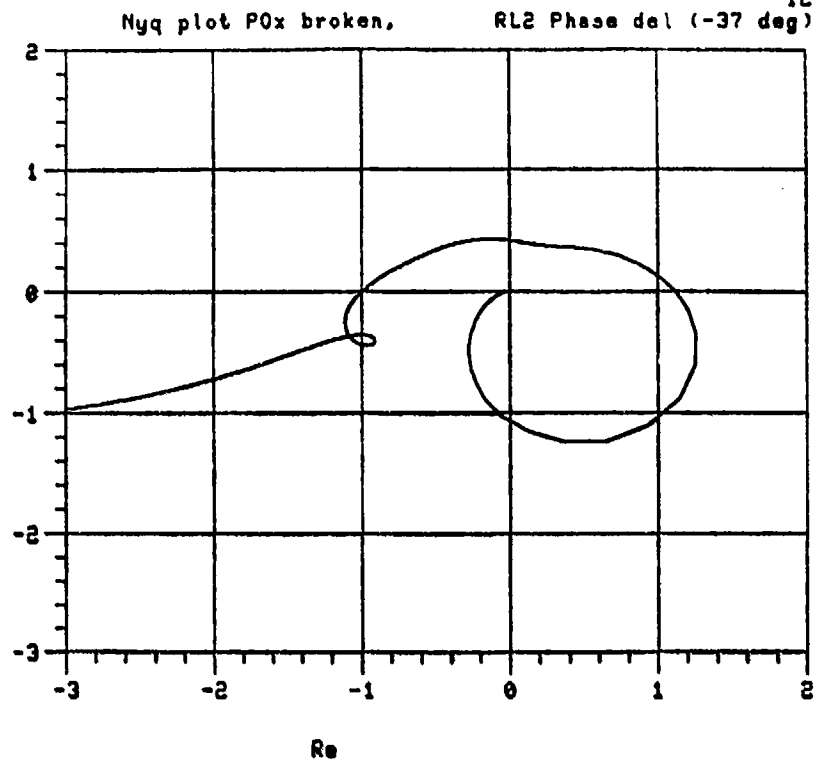


Fig. 20a: RL-2 Nyquist plot, added phase of 37 degrees

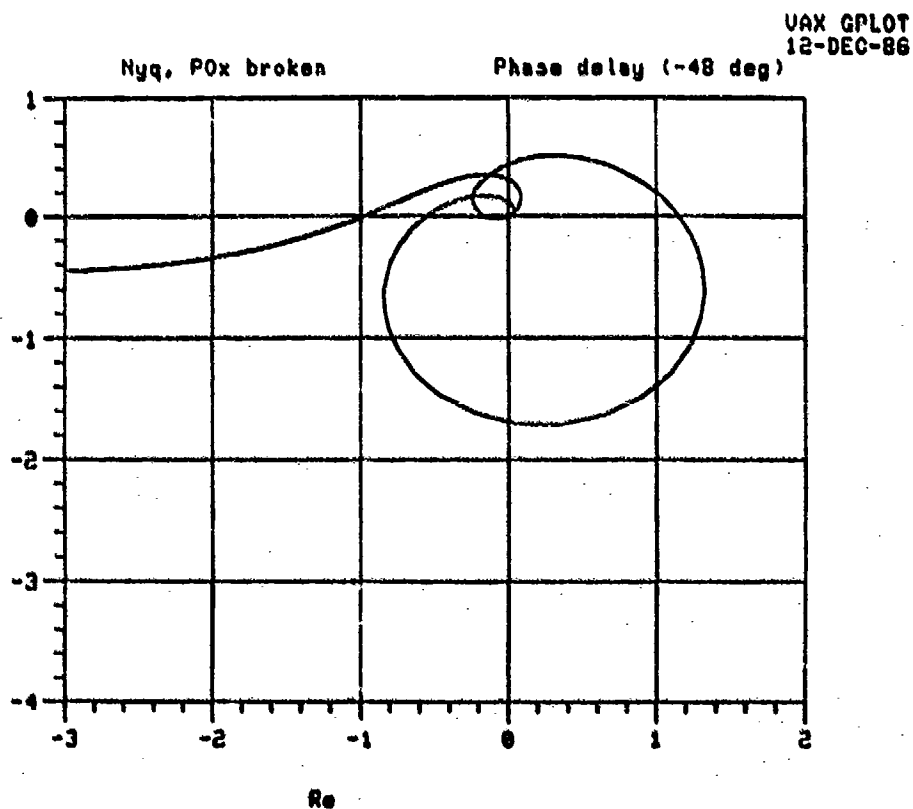


Fig. 20b: RL-3 Nyquist plot, added phase of 48 degrees

where 'b' is a positive number, and increase 'b' until the plot goes through $(-1,0)$. Note that the plots will not simply expand or rotate as they did in the classical case, but rather they will also change their shape slightly because the constants, 'a' or 'b' get embedded in the "open-loop" transfer function. It is felt that this gives a reasonable feel for the degree of stability that the closed-loop system will have. The results of this test are shown in Figures 19 and 20 and tabulated below in Table 4. The figures show the limiting cases; the smallest additional gain or phase that causes the Nyquist plot to go through $(-1,0)$.

Table 4: Stability margins

Loop	Gain Margin (db)	Phase Margin(deg)
RL-2	2.6	37
RL-3	6.8	48
RL-3 (no spin notch)	7.4	50

In Table 4, a case of RL-3 without the spin notch filter was included to show that its addition does reduce the stability margin but not significantly. It can be noted that the gain margins as calculated here are the same as were found in Section 4.1 when the root locus of the closed-loop systems as a function of p_1 (the main compensator gain) was computed since exactly the same parameter was changed here. Both of the systems have some stability margin with RL-3 being very close to what would be considered a good design by classical designers. RL-2, on the other hand, seems to lack a sufficient stability margin. This fact was recognized early in the design of the rebalance loops and was viewed as an acceptable penalty to achieve a large bandwidth in RL-2. At the present time, there is another version of RL-2 being tested that has a

significantly lower bandwidth but a much better stability margin.

There is another observation that may be made about these Nyquist plots. When additional phase was added to RL-2 or RL-3 (Fig. 20), the lobe around the origin became "stretched" - points that were close together for the nominal loop (Figure 19) became farther apart (these plots were made with the same frequency spacing). This effect seems to be an indication of reduced stability margin but it is not well understood at the present time.

In summary, the Nyquist plots indicate that both loops have reasonable stability margin, RL-3 being superior.

4.4 Effects of a Better Gyro Model

A short study of the effects of the gyro's internal damping and time constant was conducted. This involved using a more complex gyro model. The model chosen was equation (58) of [4]. This model included all damping forces in the gyro, which would cause the rotor to slowly align with the case if there were no rebalance loop around the gyro (in the ideal gyro, the rotor would never follow the case). This effect has a time constant of about 100 seconds for the CSG-2. A spin speed slightly different from the tuned speed will result in some internal torques that are not "cancelled out", creating extra dynamics. These effects are easily incorporated into the model but it is very difficult to accurately determine numerical values that approximate the real gyro without sufficient experimental data. Some crude experiments were conducted with a prototype CSG-2 to get a feel for reasonable values. These were then inserted into the model and frequency and time response simulations were rerun. The resulting figures vary insignificantly with what has been determined with the use of the simpler model. This is not surprising as the excellent stability and sensitivity properties of the closed-loop systems

have already been demonstrated. It is difficult to accurately assess the results without more gyro test data, and since the loops have good sensitivity and stability properties, a rigorous investigation was not pursued.

5 CONCLUSIONS

A combination of classical and modern control theory has been applied to analyze several important properties of the rebalance loops designed at DREO for the CSG-2 gyro. It has been determined that overall, the loops should perform very well. An examination of time responses show that the loops can handle well over 1 rad/s step rate changes and maintain the pickoff angles to less than half a degree (the rotor might hit its stops if the pickoff angle were much larger). The roll rate test showed no steady state contribution to navigation system error due to the rebalance loops. The frequency responses reveal closed-loop bandwidths of 80 to 90 Hz which should be quite adequate in dynamic environments. The sensitivity plots indicate good low frequency tracking capabilities as well as low sensitivity to parameter variations or unmodelled dynamics, except possibly in the frequency range from 30 to 120 Hz. The Nyquist plots show good stability margins that indicate the systems will remain stable under large parameter variations (2 to 7 db gain margin, 40 to 50 degree phase margin).

Several differences have been pointed out between RL-2, which employs no cross-axis compensation, and RL-3 which does. The notable advantages of RL-3 over RL-2 are: one, reduced cross-axis interaction (by a factor of 10 or more); two, elimination of the phenomenon of a steady-state acceleration on one axis creating a nonzero output on the other (in RL-2 this effect was roughly 0.001 times the magnitude of the

acceleration); and three, an increased stability margin (roughly double) for a loop of approximately the same bandwidth. The price paid by RL-3 is, one, increased circuit component count, and two, amplifier drift problems in the cross-axis amps that may add to the bias drift of the gyro. The cross-axis amps may drift because they are not caged by the integrators in the direct-axis that remove any drifts when the loops are closed.

Further testing is to be carried out to determine the necessity and/or usefulness of the cross-axis compensation, in light of the higher achievable performance and extra electronics problems involved.

6 RECOMMENDATIONS

It is recommended that the RL-3 scheme be the main loop incorporated in any prototype system that uses the CSG-2, chiefly for its superior performance in high dynamic environments. It is also suggested that an interchangeable RL-2 type loop also be kept so that a practical comparison of the two schemes can be made at the system level, i.e., effect on navigation or AHRS (attitude, heading reference system) accuracy. In this way it can be quickly determined if the higher performance or the extra electronics problems are dominant. Some attention should be paid to the performance of the loops in the 30 to 80 Hz region to ensure that the higher sensitivity in this range is not detrimental.

REFERENCES

- [1] E.W. Howe and P.H. Savet, "The dynamically tuned free rotor gyro," Control Engineering, pp. 67-72, June 1964.
- [2] M.F. Vinnins, L.D. Gallop, and F. Paquet, "Test evaluation of the Litton (Canada) Canadian Strapdown Gyroscope (CSG-2)," DREO Report 914, September 1986.
- [3] F. Paquet, "Dynamic analysis of rebalance loops," DREO Tech. memo 25/86, September 1986.
- [4] R.J.G. Craig, "Theory of operation of an elastically supported, tuned gyroscope," IEEE Trans. Aerospace and Electronic Syst., vol. AES-8, pp. 280-288, May 1972.
- [5] R.J.G. Craig, "Theory of errors of a multigimbal, elastically supported, tuned gyroscope," IEEE Trans. Aerospace and Electronic Syst., vol. AES-8, pp. 289-297, May 1972.
- [6] E.J. Davison and B.R. Copeland, "Gain margin and time lag tolerance constraints applied to the stabilization problem and robust servomechanism problem," IEEE Trans. Auto. Control, vol. AC-30, pp. 229-239, March 1985.
- [7] M.J. Chen and C.A. Desoer, "Necessary and sufficient conditions for robust stability of linear distributed feedback systems," Int. J. Control, vol. 35, pp. 255-267, 1982.

APPENDIX A

LIST OF COMPENSATOR PARAMETERS

RL-2 Parameters

0.2	P1	MAIN GAIN
31.4159	P2	INTEGRATOR CORNER FREQ (rad/s)
1255.13	P3	DEMOP LPF. CORNER FREQ (rad/s)
0.707	P4	DEMOP LPF. DAMPING
856.335	P6	NUTATION LPF. CORNER FREQ (rad/s)
0.707	P7	NUTATION LPF. DAMPING

RL-3 Parameters

0.21	P1	MAIN GAIN
31.4159	P2	INTEGRATOR CORNER FREQ (rad/s)
1332.03	P3	DEMOP LPF. CORNER FREQ (rad/s)
0.55	P4	DEMOP LPF. DAMPING
0.	P5	SPIN NOTCH DEPTH
890.956	P6	NUTATION LPF. CORNER FREQ (rad/s)
0.7	P7	NUTATION LPF. DAMPING
1.0	P8	CROSS AXIS GAIN
1036.73	P9	NUTATION NOTCH FREQ (rad/s)
0.05	PA	NUTATION NOTCH DEPTH
0.45	PB	NUTATION NOTCH DAMPING
1745.47	PC	DERIVATOR CORNER FREQ (rad/s)
0.65	PD	DERIVATOR DAMPING
662.876	PE	SPIN NOTCH FREQ (rad/s)
0.05	PF	SPIN NOTCH DAMPING

Parameters to test $C = D s^{\sim}$

0.2	P1	MAIN GAIN
31.1459	P2	INTEGRATOR CORNER FREQ (rad/s)
1255.13	P3	DEMODO LPF. CORNER FREQ (rad/s)
0.707	P4	DEMODO LPF. DAMPING
1.0	P5	SPIN NOTCH DEPTH
856.335	P6	NUTATION LPF. CORNER FREQ (rad/s)
0.707	P7	NUTATION LPF. DAMPING
1.0	P8	CROSS AXIS GAIN
929.911	P9	NUTATION NOTCH FREQ (rad/s)
1.0	PA	NUTATION NOTCH DEPTH
0.4	PB	NUTATION NOTCH DAMPING
856.335	PC	DERIVATOR CORNER FREQ (rad/s)
0.707	PD	DERIVATOR DAMPING
662.876	PE	SPIN NOTCH FREQ (rad/s)
0.05	PF	SPIN NOTCH DAMPING

Note that a notch depth (P5,PA) parameter of 1.0 means the notch filter is defeated.

SECURITY CLASSIFICATION OF FORM
(highest classification of Title, Abstract, Keywords)

DOCUMENT CONTROL DATA

(Security classification of title, body of abstract and indexing annotation must be entered when the overall document is classified)

1. ORIGINATOR (the name and address of the organization preparing the document. Organizations for whom the document was prepared, e.g. Establishment sponsoring a contractor's report, or tasking agency, are entered in section B.) Defence Research Establishment Ottawa Dept. National Defence Ottawa, Canada K1A 0Z4		2. SECURITY CLASSIFICATION (overall security classification of the document including special warning terms if applicable) <p align="center">UNCLASSIFIED</p>	
3. TITLE (the complete document title as indicated on the title page. Its classification should be indicated by the appropriate abbreviation (S,C,R or U) in parentheses after the title.) An Analysis of DREO's Analog Rebalance Loops for the CSG-2 Tuned-Rotor Gyroscope. (U)			
4. AUTHORS (Last name, first name, middle initial. If military, show rank, e.g. Doe, Maj. John E.) Bird, Jeffrey S.			
5. DATE OF PUBLICATION (month and year of publication of document) July 1987		6a. NO. OF PAGES (total containing information. Include Annexes, Appendices, etc.) 58	6b. NO. OF REFS (total cited in document) 7
7. DESCRIPTIVE NOTES (the category of the document, e.g. technical report, technical note or memorandum. If appropriate, enter the type of report, e.g. interim, progress, summary, annual or final. Give the inclusive dates when a specific reporting period is covered.) Technical Note			
8. SPONSORING ACTIVITY (the name of the department project office or laboratory sponsoring the research and development. Include the address.) N/A			
9a. PROJECT OR GRANT NO. (if appropriate, the applicable research and development project or grant number under which the document was written. Please specify whether project or grant) 041LJ		9b. CONTRACT NO. (if appropriate, the applicable number under which the document was written) N/A	
10a. ORIGINATOR'S DOCUMENT NUMBER (the official document number by which the document is identified by the originating activity. This number must be unique to this document)		10b. OTHER DOCUMENT NOS. (Any other numbers which may be assigned this document either by the originator or by the sponsor)	
11. DOCUMENT AVAILABILITY (any limitations on further dissemination of the document, other than those imposed by security classification) (X) Unlimited distribution () Distribution limited to defence departments and defence contractors; further distribution only as approved () Distribution limited to defence departments and Canadian defence contractors; further distribution only as approved () Distribution limited to government departments and agencies; further distribution only as approved () Distribution limited to defence departments; further distribution only as approved () Other (please specify):			
12. DOCUMENT ANNOUNCEMENT (any limitation to the bibliographic announcement of this document. This will normally correspond to the Document Availability (11). However, where further distribution (beyond the audience specified in 11) is possible, a wider announcement audience may be selected.) Unlimited			

UNCLASSIFIED

SECURITY CLASSIFICATION OF FORM

13. ABSTRACT (a brief and factual summary of the document. It may also appear elsewhere in the body of the document itself. It is highly desirable that the abstract of classified documents be unclassified. Each paragraph of the abstract shall begin with an indication of the security classification of the information in the paragraph (unless the document itself is unclassified) represented as (S), (C), (R), or (U). It is not necessary to include here abstracts in both official languages unless the text is bilingual).

The Defence Research Establishment Ottawa (DREO) designed and constructed a high performance analog rebalance loops for the Canadian Strapdown Gyroscope (CSG-2). This instrument is a potentially low cost, near inertial grade, two degree-of-freedom, tuned-rotor gyro designed and manufactured by Litton Systems Canada Ltd. under contract to DREO. The resulting loops are analyzed extensively from a control systems point of view with the examination of such properties as closed-loop stability margin, as interpreted from multivariable generalizations of classical control-theoretic notions of Nyquist plots and root locii. The results indicate that the loops will provide sufficient closed-loop performance to achieve the desired goals of bandwidth, maximum input rate, low cross-axis coupling and acceleration compensation.

14. KEYWORDS, DESCRIPTORS or IDENTIFIERS (technically meaningful terms or short phrases that characterize a document and could be helpful in cataloguing the document. They should be selected so that no security classification is required. Identifiers, such as equipment model designation, trade name, military project code name, geographic location may also be included. If possible, keywords should be selected from a published thesaurus, e.g. Thesaurus of Engineering and Scientific Terms (TEST) and that thesaurus identified. If it is not possible to select indexing terms which are Unclassified, the classification of each should be indicated as with the title.)

Rebalance Loop
Gyroscopes
Tuned-Rotor Gyroscope
Strapdown Gyroscope
Two-Degree-of-Freedom Gyroscope
Inertial Navigation Sensors
Control Systems Applications

UNCLASSIFIED

SECURITY CLASSIFICATION OF FORM